DMD Fast Forward. Published on July 24, 2008 as doi:10.1124/dmd.108.022277

DMD #22277

Metabolism, Pharmacokinetics and Excretion of a Cholesteryl Ester Transfer Protein Inhibitor, Torcetrapib, in Rats, Monkeys, and Mice: Characterization of Unusual and Novel Metabolites by High Resolution LC-MS/MS and ^{1}H NMR

Chandra Prakash, Weichao Chen, Michelle Rossulek, Kim Johnson, Chenghong Zhang, Thomas O'Connell, Michael Potchoiba and Deepak Dalvie

Departments of Pharmacokinetics, Dynamics and Metabolism, Pfizer Global Research and Development, Groton, CT 06340

DMD Fast Forward. Published on July 24, 2008 as DOI: 10.1124/dmd.108.022277
This article has not been copyedited and formatted. The final version may differ from this version.

DMD #22277

IN VIVO METABOLISM OF TORCETRAPIB IN PRECLINICAL SPECIES

Address for Correspondence:

Chandra Prakash, Ph. D.
Pharmacokinetics, Dynamics and Metabolism
Pfizer Global Research and Development
Groton, CT 06340
Ph. No. 860-441-6415
Fax No. 860-686-0654
Email: Chandra.prakash@pfizer.com

Abstract	233
Introduction	518
Discussion	1423
Text pages	51
Tables	8
Figures	17
References	30

[1]Abbreviations: CHD, coronary artery disease; CETP, (cholesteryl ester transfer protein); SD, Sprague-Dawley;; MCID, MicroComputer Imaging Device; radio-HPLC, HPLC with on-line radioactivity detector; LC-MS/MS, liquid chromatography-tandem mass spectrometry; β̃-RAM, radioactive monitor; CID, collision induced dissociation; LSC, liquid scintillation counting; BTFMBA, bis-trifluoromethylbenzoic acid; HPD, hours postdose.

Abstract

The disposition of torcetrapib, a CETP inhibitor, was studied in rats, monkeys and mice following oral administration of a single dose of [^{14}C]torcetrapib. Total mean recoveries of the radiocarbon were 90.9, 93.4 and 86.8% from mice, rats, and monkeys, respectively. Excretion of radioactivity was rapid and nearly complete within 48 h after dosing with majority excreted in the feces in all species. Torcetrapib was not detected in the urine and/or bile across species suggesting that it is primarily cleared by metabolism in these species. More than twenty eight metabolites were identified in all species, and were products of oxidation and conjugation pathways. The primary metabolic pathways of torcetrapib involved hydrolysis of the carbamate ester (M2) and the oxidation of the ethyl moieties. M2 was subsequently metabolized in parallel by oxidative cleavage to novel and unusual quinoline metabolites (M3, M4, M5, M9 and M17), bis trifluuromethyl benzoic acid (M1), and 3,5 bis(trifluoromethyl)phenyl)-(methoxycarbonyl)methanesulfonic acid (M28). The structures of several metabolites were established by high resolution LC-MS/MS and ^{1}H NMR. The major circulating and excretory metabolites in mice, rats and monkeys were species-dependent, however, several common metabolites were observed in more than one species. In addition to parent torcetrapib, M1, M3, and M4 in rats, M4 and M17 in mice, and M3 and M8 in monkeys were detected as the major circulating metabolites. A mechanism for the formation of an unusual metabolite M28 has been proposed.

DMD Fast Forward. Published on July 24, 2008 as DOI: 10.1124/dmd.108.022277
This article has not been copyedited and formatted. The final version may differ from this version.

Although low-density lipoprotein-cholesterol (LDL-C)-lowering statins therapies have shown consistent benefit for reduction the mortality and morbidity associated with coronary artery disease (CHD[1]) (Schaefer and Brousseau 2000), there still remain a significant number of patients for which these therapies have not prevented events due to cardiovascular disease (Shepherd et al., 1995; Sacks, et al., 1996; Downs et al., 1998). In addition to high levels of LDL-C, low levels of high-density lipoprotein cholesterol (HDL-C) are also a strong and independent risk factor for the incidence of CHD (Barter et al., 2003). Plasma concentrations of HDL-C are regulated in part by production of nascent HDL particles, primarily by the liver and intestine, and by the actions of a series of plasma enzymes and transfer proteins, including lipoprotein and hepatic lipase, lecithin-cholesterol acyltransferase, and CETP (Bruce et al., 1998). The effects of CETP activity on plasma lipoproteins and atherosclerosis have been examined in animal models and human subjects (Marotti et al., 1993; Plump et al., 1999; Whitlock et al., 1989; Evans et al., 1994; Gaynor et al., 1994; Inazu et al., 1990; Teh et al., 1998). These studies seem to suggest that while total elimination of CETP activity may not necessarily afford a benefit, at least the partial inhibition of CETP appears to provide a reduction in atherosclerosis and CHD risk. Thus a number of academic and industrial enterprises have pursued a pharmacological inhibitor of CETP to reduce the morbidity and mortality associated with cardiovascular diseases.

Torcetrapib{(–)-[2R,4S] 4-[(3,5-*bis*-trifluoromethylbenzyl)-methoxycarbonyl-amino]-2-ethyl-6-trifluoromethyl-3,4-dihydro-2H-quinoline-1-carboxylic acid ethyl ester}, a CETP inhibitor, was being developed in combination with atorvastatin as a means of reducing cardiovascular risk by increasing levels of HDL-C and reducing levels of LDL-C (Clark et al., 2006). In Phase 2 studies, administration of torcetrapib has resulted in dose-dependent increases in plasma HDL

and decreases in plasma LDL concentrations. However, development of torcetrapib was discontinued following an excess in mortality in the active treatment arm of the study (Howes and Kostner, 2007). The underlying cause of this imbalance remains undetermined.

Preclinical pharmacokinetic studies in nonclinical species suggested that torcetrapib is well absorbed and readily distributed throughout the body tissues. Metabolic pathways of drug candidates in animals, used for safety evaluation studies, are required to ensure that the selected animal species are exposed to all major metabolites formed in humans (FDA, 2008). Recently, FDA suggested that additional toxicological testing on metabolites that have higher exposure in humans than preclinical species may be required (FDA, 2008). The objectives of the present study were to characterize the disposition of torcetrapib in rats, mice and monkeys and to identify and quantify its excretory and circulating metabolites. A single dose of [^{14}C]torcetrapib was orally administered to intact and bile-duct cannulated SD rats (20 mg/kg) and Cynomolgus monkeys (60 mg/kg), and intact mice (20 mg/kg). The urine, bile/feces and plasma were collected and assayed for radioactivity, and profiled for metabolites. The metabolites were separated on reverse phase HPLC and analyzed by high resolution LC/MS and LC/MS/MS, and where possible, the proposed structures were supported by proton NMR and by comparisons of their HPLC retention times and MS spectra with those of synthetic standards.

Materials and method

General Chemicals. Commercially obtained chemicals and solvents were of HPLC or analytical grade. Zorbox C-18 HPLC analytical and preparative columns were obtained from Phenomenex (Torrance, CA). Ecolite (+) scintillation cocktail was obtained from ICN (Irvine, CA). Carbosorb and Permafluor E+ scintillation cocktails were purchased from PerkinElmer Life and

Analytical Sciences (Boston, MA). HPLC grade acetonitrile, methanol and water, and certified ACS grade ammonium acetate and acetic acid were obtained from Fisher Scientific Company (Springfield, NJ).

Radiolabeled Drug and Reference Compounds. [^{14}C]torcetrapib-A, labeled at the C-4 position of the trifluoromethyl-3,4-dihydro-2H-quinoline moiety (specific activity, 58 mCi/mmol) and [^{14}C]torcetrapib-B, labeled at the benzylic position of the bis-trifluorophenyl ring (specific activity, 56 mCi/mmol) were synthesized by the radiochemistry group at Pfizer Global Research and Development (Groton, CT) (Fig.1). Both showed a radiochemical purity of ≥98%, as determined by HPLC using an in-line radioactivity detector and characterized by MS and NMR. The synthetic reference compounds standards, 6-(trifluoromethyl) quinoline-2-carboxylic acid, 6-trifluoromethyl-2-methyl quinoline, 6-(trifluoromethyl) quinolin-2-yl methanol and 3,5-bis(trifluoromethyl)phenyl)-(methoxycarbonyl-amino)methanesulfonic acid were synthesized at Pfizer Global Research and Development (Groton, CT) using standard procedures (Damon et al., 2006).

Animals, Dosing and Sample Collection. Intact, bile-duct or jugular vein cannulated SD rats (190-270 g) and mice (25-30 g) were purchased from Charles River Laboratories (Stoneridge, NY). Cynomolgous monkeys (4-6 kg) were from an established in house colony. Animals were quarantined for a minimum of 3 days prior to treatment and maintained on a 12-h light/dark cycle. The animals were fasted overnight prior to administration of the dose and were fed 6 h after the dose. The animals were provided water *ad libitium*. All studies were conducted in a research facility accredited by the association for the assessment and accreditation of laboratory animal care international (AAALAC). All animal studies were approved by the institutional animal care and use committee (IACUC).

DMD Fast Forward. Published on July 24, 2008 as DOI: 10.1124/dmd.108.022277
This article has not been copyedited and formatted. The final version may differ from this version.

Rats. A group of six non-cannulated (n=3/gender) SD rats was housed individually in stainless steel metabolism cages. A single dose [^{14}C]torcetrapib-A was administered orally at a target dose level of 20 mg/kg and 120 μCi of radio carbon. The dose was formulated in a mixture of olive oil/ cremophore EL/water (40:10:50) at a target concentration of 5 mg/ml. Urine was collected into containers at 0-8, 8-24, and at 24 h intervals during the study through 168 h post-dose. The feces was collected over 24 h intervals up to 168 h post-dose. The total weight of the urine and feces was recorded after each collection. The samples were stored at - 20°C until the day of analysis.

For biliary excretion experiments, another group of two male and two female bile-duct cannulated rats was administered a single 20-mg/kg oral dose of [^{14}C]torcetrapib-A as described above. Bile was collected from male rat #1 over 0-48 h post-dose and for 0-24 h from male rat #2, female #3 and female #4 (the cannulae of rats 2, 3 and 4 came out after 24 h). The bile samples were stored at -20° C until analysis.

For pharmacokinetic experiments, a third group of jugular-vein cannulated SD rats (N=3/gender) were administered a single oral 20 mg/kg dose of [^{14}C]torcetrapib-A as described above. Blood (0.6 ml) was collected from each rat via the jugular vein in heparinized tubes at pre-dose, 0.5, 1, 2, 4, 8, 12, 24, and 48 h post-dose. A fourth group of animals (n=2/sex) was dosed for the identification of circulating metabolites. Blood was collected in heparinized tubes by decapitation of one male and one female at 4 and 6 h post dose. Blood samples were centrifuged at 1000 g for 10 min to obtain the plasma. Plasma was transferred to clean tubes and stored at -20 ^{o}C until analysis.

A fifth group of six non-cannulated (n=3/gender) SD rats was administered a single 20 mg/kg oral dose of [^{14}C]torcetrapib-B to determine the fate of bis-trifluoromethylbnzoic acid formed

DMD Fast Forward. Published on July 24, 2008 as DOI: 10.1124/dmd.108.022277
This article has not been copyedited and formatted. The final version may differ from this version.

by N-dealkylation of the trifluoromethyl-3,4-dihydro-2H-quinoline moiety of torcetrapib. Urine and feces were collected form each up to 168 h post-dose as described earlier. A sixth group of 2 male and 2 female rats was administered a single 20 mg/kg oral dose of [^{14}C]torcetrapib-B for identification of circulating metabolites. Blood samples were collected from two rats (one male and one female) at 2 and 8 h postdose. Plasma was separated and stored at -20 ^{O}C until analysis.

Monkeys. Four (two male and two female) intact and two (male) bile-duct cannulated Cynomolgous monkeys (3-4 kg) were housed individually in stainless steel metabolism cages. A single dose of [^{14}C] torcetrapib-A was administered orally at a target dose level of 60 mg/kg (~150 μCi/animal). The dose was formulated in a mixture of miglyol 812 (84 ml), propylene carbonate (28 ml), and Cremophore EL (28 ml) and milli-Q water (92.5 ml) at a target concentration of 12 mg/ml on the day of the dose administration. Urine was collected into containers surrounded by dry-ice at predose (-12-0), 0-8, 8-24, and at 24 h intervals during the study through 192 h post-dose. The feces was collected over predose (-12-0), and then over 24 h intervals, up to 192 h post-dose. Urine, bile and feces were collected from bile-duct cannulated monkeys at predose (-12-0), 0-24 and 24-48 h post-dose. The total weight of the urine, bile and feces was recorded after each collection. Blood samples (5 ml) were collected from the vascular access port (VAP) or via venipuncture of a peripheral vessel in heparinized tubes at pre-dose, 0.5, 1, 2, 4, 8, 12, 24, h post dose and 24 h intervals through 168 h post-dose. Cage debris was collected after each fecal collection and the cage floors, screens and pans were rinsed with aqueous ethanol (50%). After the last urine and fecal collection, the cages were washed with aqueous ethanol (50%) and the washes were collected.

Mice. A group of nine male and nine female CD-1 mice (25-31 g) were housed in Nalgene metabolism cages (3 mice/cage) designed to collect urine and feces. Each animal was administered a single oral 20 mg/kg, dose of [^{14}C]torcetrapib-A. The ^{14}C dose was formulated at a target concentration of 2 mg/ml in Cremaphor EL/olive oil/water (1/4/5, v/v). Urine and feces were collected from these animals for 7 days at 0-8, 8-24, 24-48, 48-72, 72-96, 96-120, 120-144 and 144-168 h post-dose. For circulating metabolites identification four groups of three animals per sex were a single oral 20 mg/kg, dose of [^{14}C]torcetrapib-A. Blood was collected from three animals/gender in heparinized tubes at 2, 4, 6 and 8 h post-dose. For pharmacokinetics, eight groups of three animals per sex were administered a single oral dose of 20 mg/kg, dose of [^{14}C]torcetrapib-A. Whole blood was collected from three animals /gender in heparinized tubes at 30 min, 1, 2, 4, 8, 12, 24, and 48 h post dose. Plasma was separated from whole blood by centrifugation and stored at –20°C until use.

Determination of Radioactivity. Radioactivity in plasma, urine, bile and feces was measured by liquid scintillation counting. Aliquots of plasma (25-100 µl, in duplicate), urine (100-500 µl, in triplicate) and bile (100µl, in triplicate) for each sampling time from all animals were mixed with 15 ml of Ecolite (+) scintillation cocktail and counted in a Wallac 1409 (GE Healthcare, Chalfont St. Giles, Buckinghamshire, UK) or a Model LS 6000 (Beckman, Fullerton, CA) liquid scintillation counter. For determination of radioactivity in feces, the weight of each fecal sample was determined and the samples were homogenized in deionized water using a probe-type homogenizer. Following homogenization, triplicate aliquots (0.1-0.5 g) of each homogenate were transferred into tared cones and pads, air dried before combustion in an automatic sample oxidizer (PerkinElmer oxidizer 308; Boston, MA). Radioactivity in the combustion products was determined by trapping the liberated CO_2 in Carbo-sorb followed by liquid scintillation

counting using Permafluor E+ as a scintillation cocktail. Combustion efficiency was determined daily, prior to the combustion of study samples, using diluted dose formulation or a carbon-14 standard. The measured radioactivity content in combusted samples was adjusted using the combustion efficiency values. Samples were analyzed for radioactivity for 2 min (5 or 10 min for plasma). Scintillation counter data were automatically corrected for counting efficiency using an external standardization technique and an instrument-stored quench curve generated from a series of sealed quench standards. Radioactivity less than twice the background value was considered to be below the limit of determination

Samples collected prior to dosing were used as controls and counted to obtain a background count rate. Radioactivity in the dose was expressed as 100% and the radioactivity in urine, bile and feces at each sampling time was defined as the percentage of dose excreted in the respective matrices at that sampling time. The amount of radioactivity in plasma was expressed as nanogram-equivalents of torcetrapib per mililiter and was calculated by using the specific activity of the dose administered.

Extraction of Metabolites from Biological Samples. Urine from 0-72 h for both rats and monkeys and 0-48 h for mice was pooled proportional to the volumes of urine collected at each time point. The pooled urine accounted for greater than 90% of the excreted radioactivity. The pooled urine samples were then centrifuged (1000 x g for 10 min) and the aliquots (~100 μl) of supernatants were directly injected onto the HPLC column without further purification.

An aliquot of bile (0-24 h) was diluted with 4 volumes of acetonitrile and the precipitated material was removed by centrifugation. The pellet was washed with an additional one volume of acetonitrile and both supernatants were combined. The extraction recovery of the radioactivity in bile was about 85% after extraction. The supernatant was evaporated to dryness

under nitrogen in a Turbo Vap LV evaporator (Caliper life sciences, Hopkinton, MA) and the residue was re-dissolved in 20:80 acetonitrile: 10 mM ammonium formate (pH 3.0). An aliquot was injected onto the HPLC column.

The fecal homogenates were pooled from 0-48 h for rats and mice and 0-72 h for monkeys so that 90% or greater radioactivity was accounted for. From the pooled samples, aliquots (~10-12 g) were suspended in 30 ml of acetonitrile. Suspensions were sonicated (~30 min.), vortexed and centrifuged at 1000 x g for 10 min. Following supernatant transfer to clean conical tubes, the residues were further extracted 3 times with 30 ml of acetonitrile as described above. Aliquots (100 µl) from the pooled extracts were counted in a liquid scintillation counter. The recovery of radioactivity extracted ranged from 85-96%. The supernatants were evaporated in a turbovap LV evaporator at 35 °C under nitrogen. The residues obtained were reconstituted in 1-2 ml of acetonitrile/H_2O and aliquots (100 µl) were injected onto the HPLC column.

Rat and mouse plasma obtained for metabolite profiling and identification was diluted with 3 volumes of acetonitrile. The mixture was then centrifuged and the supernatant was transferred to a clean tube. The pellet was extracted with an additional 2 ml of acetonitrile. Both supernatants were combined and an aliquot was counted in a scintillation counter. The extraction recovery of the radioactivity in plasma was >80%. The supernatant was evaporated in a turbovap at 35 °C under nitrogen. The residue was reconstituted in mobile phase (see below) and injected onto the LC-MS/MS.

For monkeys, plasma (3 ml pooled; equal volume of each time point) was diluted with 9 ml of acetonitrile and the precipitated protein was removed by centrifugation. The pellets were extracted with an additional 2 ml of acetonitrile. The extraction recovery of the radioactivity in plasma was 80-88%. The supernatants from the two extractions were combined and

concentrated under nitrogen in a Turbo Vap LV evaporator. The residues were reconstituted in 500 µl of HPLC mobile phase and aliquots (100 µl) were injected onto the LC-MS/MS column without further sample purification.

Chromatography. The HPLC system consisted of an HP-1100 solvent delivery system, an HP-1100 membrane-degasser, an HP-1100 autoinjector from Hewlett Packard (Palo Alto, CA), and an IN/US ß-RAM radioactivity monitor (IN/US, Tampa, FL). Chromatography was performed on a Zorbax C18 column (5 micron, 4.5 x 150 mm) with a mobile phase containing a mixture of) and 10 mM ammonium formate (pH 2.0; solvent A) and acetonitrile (solvent B). For urine and plasma of rats and monkeys, the mobile phase was initially composed of solvent A/solvent B (95:5), and held for 5 min. The mobile phase composition was then linearly programmed to solvent A/solvent B (60:40), over 10 min and then changed to solvent A/solvent B 40:60 over 13 min. A short gradient was programmed to solvent A/solvent B (5:95) over 2 min and the mobile phase composition was returned to the starting solvent mixture over 5 min. The system was allowed to equilibrate for approximately 15 min before making the next injection. The flow rate was 1.0 ml/min and the separation was achieved at ambient temperature.

For separation of biliary metabolites, the mobile phase was initially composed of solvent A/solvent B (80:20), held isocratic for 5 min, then ramped to 20:80 over 35 min, followed by another ramp to 5:95 over 10 min. The system was returned to starting solvent mixture over 2 min and was allowed to equilibrate for 8 min prior to the next injection.

For separation of fecal and plasma metabolites of mice, chromatography was performed on an Agilent C-18 SB column (4.6 mm x 150 mm, 5 µm) with a mobile phase containing a mixture of 10 mM ammonium formate pH 3.0 (solvent A) and acetonitrile (solvent B). The mobile

phase was initially composed of solvent A/solvent B (80:20), held for 5 min and was then linearly programmed to solvent A/solvent B (20:80), over 35 min. A gradient was programmed to solvent A/solvent B (5:95) over 10 min and the mobile phase composition was returned to the starting solvent mixture over 2 min. The system was allowed to equilibrate for approximately 10 min before making the next injection. The flow rate was 1.0 ml/min and the separation was achieved at ambient temperature. . Due to co-eluting peaks in the urine samples using the pH 3.0 formate buffer, urine samples were profiled using the exact conditions as stated above, except that the solvent A consisted of ammonium formate at pH 6.4.

For separation of urinary metabolites of rats dosed with [^{14}C]torcetrapib-B, C-14 labeled at the benzylic position, the mobile phase was initially composed of solvent A/solvent B (90:10), and held for 5 min. The mobile phase composition was then linearly programmed to solvent A/solvent B (70:30), over 5 min and then changed to solvent A/solvent B 30:70 over 20 min. A short gradient was programmed to solvent A/solvent B (15:85) over 5 min and to solvent A/solvent B (10:90) over 5 min. The mobile phase composition was returned to the starting solvent mixture over 5 min. The system was allowed to equilibrate for approximately 15 min before making the next injection. The flow rate was 1.0 ml/min and the separation was achieved at ambient temperature.

Quantitative Assessment of Metabolites. Quantification of the metabolites was carried out by measuring radioactivity in the individual HPLC-separated peaks using a β-RAM. The β-RAM provided an integrated printout in counts per minute and percentage of the radiolabelled material, as well as peak representation. The β-RAM was operated in the homogeneous liquid scintillation counting mode, with addition of 3 ml/min of Tru-Count scintillation cocktail to the effluent post UV detection. For the quantification of plasma metabolites of mice, the HPLC

effluent was directed into the flow cell of a β-ram radioactivity detector. The β-ram and HPLC apparatus were controlled externally using an Accurate radioisotope counting (AIM Research, Hockessin, DE) system, for low-level radioactivity counting.

LC-MS/MS. LC-MS/MS was conducted with a PE-Sciex API 2000 (PerkinElmerSciex Instruments; Boston, MA), a Micromass Q-TOF (Waters; MA) or a Finnigan LCQ Ion Trap (Thermoelectron, Waltham, MA) equipped with an electrospray ion source .The effluent from the HPLC column was split and about 50 µl/min was introduced into the atmospheric ionization source. The remaining effluent was directed to the flow cell of β-RAM. The β-RAM response was recorded as a real time analog signal by the MS data collection system. This allowed simultaneous real time monitoring of radioactivity and the detection of the total ion chromatogram. All mass spectrometers were, unless mentioned otherwise, operated in the positive ion mode. Data were collected in the Q1 scanning, neutral loss scanning, precursor ion scanning, product ion scanning, multiple reaction monitoring scanning and data dependant ion scanning modes, with instrument settings and potentials (e.g. collision energy) adjusted to provide optimal data in each mode. Additional metabolite identification and verification was performed by elemental composition determination using the Micromass q-TOF. Lock mass for the q-TOF was achieved by infusing quinidine at 325.1916 Da for accurate mass determination calculations.

LC-MS-NMR. LC-MS-NMR system was consisted of an Agilent 1100 binary pump, membrane-degasser and auto injector (Agilent Technologies, Palo Alto, CA), a Bruker BioSpin BSFU-0 column oven (Bruker BioSpin Corporation, Billerica, MA), a Bruker BioSpin photodiode array detector, a Bruker BioSpin BNMI interface using a 20:1 split, a Bruker Daltonics Esquire 3000 ion trap MS (Bruker Daltonics Inc., Billerica, MA) equipped with an

electrospray source, a Bruker BioSpin BPSU-36 peak storage unit, and a Bruker BioSpin 500 MHz Avance DRX Spectrometer equipped with a 4 mm 1H-13C inverse z-gradient LC flow probe. Proton chemical shifts (δ) are reported in ppm relative to tetramethylsilane as referenced from the shift of residual protons in MeCN-d3 (1.94 ppm). Chromatography for M4 was performed on a Zorbax C8 Rx column (5 micron, 4.6 x 150 mm) with a mobile phase containing a mixture of (0.1% TFA-d in D2O) (solvent A) and MeCN-d3 (solvent B) The mobile phase was initially composed of solvent A/solvent B (80:20) was then linearly programmed to solvent A/solvent B (60:40), over 40 min. The flow rate was 1.0 ml/min and the separation was achieved at ambient temperature. Chromatography for M28 was performed on a Develosil C30 column (3 micron, 3.0 x 150 mm) with a mobile phase containing a mixture of (15 mM AcOD-d4 in D2O; pH 5) (solvent A) and MeCN-d3 (solvent B) The mobile phase was initially composed of solvent A/solvent B (80:20) was then linearly programmed to solvent A/solvent B (50:50), over 60 min. The flow rate was 0.5 ml/min and the separation was achieved at ambient temperature.

Quantitation of Torcetrapib: The plasma samples were analyzed for unchanged torcetrapib using PerkinElmer SCIEX API 3000 (PerkinElmer-Sciex Instruments; Boston, MA). A 100 µl aliquot of each plasma sample containing torcetrapib was treated with 10 µl of 1 µg/ml internal standard, a structure analog of torcetrapib, (2S,4S)-isopropyl 2-cyclopropyl-4-(methoxycarbonyl)-6-(trifluoromethyl)-3,4-dihydro-2H-quinoline-1-carboxylate, and extracted on a Varian C18 (25 mg) microtiter packed bed. The bed was washed with acetonitrile:water mixture (1:1) and the analytes were eluted with 200 µl of acetonitrile and injected onto a LC/MS/MS system for analysis. The internal standard and torcetrapib were separated chromatographically using a Keystone C-8 (4.6 x 30 mm) analytical column at ambient

temperature. The mobile phase of 80% acetonitrile and 20% 10 mM ammonium acetate was used to separate the internal standard and tocetrapib in the plasma. The total run time for each sample was 3.5 min with a flow rate of 0.5 ml/min. The retention times of torcetrapib and the internal standard were 1.52 and 1.67 min, respectively. The compounds were detected in a negative ion mode using a turbo ion spray source at *m/z* 659.2 and 685.2 for torcetrapib and internal standard, respectively. Data collection and integration was done on Sciex Software sample control and Mac Quan (version 1.6), respectively. The ratio of peak area responses of drug relative to internal standard was used to construct a standard curve using a linear least square regression with a 1/x weighting. The dynamic range of the assay was 25 to1000 ng/ml. The performance of the assay was monitored by inclusion of quality control samples prepared in monkey plasma.

Pharmacokinetic Analysis. Pharmacokinetic parameters were determined using the WinNonlin-Pro Ver. 2.1 program (Pharsight, Mountain View, CA) by non-compartmental analysis. For estimation of the means and pharmacokinetic parameters, concentrations at the 0 hr and those <25.0 ng/ml were assumed to be 0 ng/ml. The means were calculated only if greater than 50% of the data were >LLOQ.

Results

^{14}C Excretion. Rats. After oral administration of a single 20 mg/kg dose of [^{14}C]torcetrapib-A to SD rats, an overall mean of 93.4 % of the total dose was recovered in the urine, feces and cage wash of the rats, over a period of 168 h postdose (Table 1). The mean percentage of dose excreted in male and female rats was 94.8 and 91.9%, respectively. The mean cumulative dose recovered in feces of male and female rats was 59.1 and 52.7 %, respectively. The mean

cumulative excretion in the urine of male and female rats was 21.3 and 21.6 % of the dose (Table 1). There was no gender difference in the routes of excretion of torcetrapib radioactivity..

Following a single oral administration of [^{14}C]torcetrapib-B, labeled at the benzylic position, an overall mean of 94.4% of the total dose was recovered in the urine, feces and cage rinse of the rats. The mean cumulative dose recovered in feces of male and female rats was 62.6 and 56.4%, respectively. The mean cumulative excretion in the urine of male and female rats was 21.1 and 21.7% of the dose (Table 1).

Monkeys. After a single oral administration of [^{14}C]torcetrapib-A, a mean of 86.8% of the total dose was recovered in the urine, feces and cage wash of the monkeys (Table 1). The cumulative dose recovery in feces of male and female monkeys ranged from 31.4 to 59.8% (mean 44.5%). The cumulative excretion in the urine of monkeys ranged from 6.59 to 45.6% (mean 29.2%).

Mice. After a single oral dose of [^{14}C]torcetrapib-A to mice, equal amounts of radioactivity were recovered in urine and feces. Urine accounted for 41.2 and 40.6% of the dose, respectively, in male and female mice (Table 1). Feces accounted for 44.3 and 40.0% of the dose in males and females, respectively (Table 1). Including the radioactivity recovered in the cage wash and carcass, approximately 90.7% of the radioactivity was recovered in CD-1 mice

Pharmacokinetics. Rats. Mean plasma concentration versus time curves of torcetrapib and total radioactivity after a single 20 mg/kg oral dose of [^{14}C]torcetrapib-A to rats are shown in fig. 2. The exposure ($AUC_{0-\infty}$) to torcetrapib in female rats was 2.3 fold greater than that in male rats. Similarly, the exposure ($AUC_{0-\infty}$) to total radioactivity in female rats was 1.6 fold greater than that in male rats. The mean C_{max} of torcetrapib in male and female rats was 1590 and 2220

ng/ml, respectively and the mean $AUC_{0-\infty}$ of torcetrapib in male and female rats was 6490 and 15000 ng·h/ml, respectively (Table 2). The mean C_{max} and $AUC_{0-\infty}$ of total circulating radioactivity in the male rats were 3020 ng-Eq/mL and 49400 ng Eq·h/ml, respectively, and the mean C_{max} and $AUC_{0-\infty}$ in the female rats was 4150 ng Eq/ml and 80700 ng Eq·h/ml, respectively (Table 3). Based on $AUC_{0-\infty}$, 13 to 19%, of the circulating radioactivity in rats was attributable to unchanged torcetrapib. The mean T_{max} of torcetrapib and total radioactivity in rats was 2.7 and 6 h, respectively. The mean terminal elimination $t_{1/2}$ of torcetrapib and total radioactivity in rats was 3.5 and 9.6 h respectively (Tables 2 and 3).

Monkeys. Mean plasma concentration versus time curves of torcetrapib and total radioactivity after a single 60 mg/kg oral dose of [^{14}C]torcetrapib-A to monkeys are shown in fig. 3. The mean C_{max} of torcetrapib and the total circulating radioactivity was 893 ng/ml (336.0 to 1270 ng/ml) and 6190 ng Eq/ml (3110 to 12100 ng Eq/ml), respectively (Tables 2 and 3). The mean T_{max} of torcetrapib and the total circulating radioactivity was 10.4 h (4 to 24 h) and 17.6 h (4.0 to 24 h), respectively. The mean $AUC_{(0-\infty)}$ of torcetrapib and the total circulating radioactivity was 50000 ng·h/ml (23000 to 73100 ng·h/ml) and 295000 ng Eq·h/ml (98500 to 533000 ng Eq·h/ml), respectively (Tables 2 and 3). The percentage of $AUC_{(0-\infty)}$ of total drug-related material that is represented by unchanged torcetrapib was 17%. The mean terminal elimination half-life of torcetrapib and the total circulating radioactivity was 99 and 80 h, respectively.

Mice. Mean plasma concentration versus time curves of torcetrapib and total radioactivity after a single 20 mg/kg oral dose of [^{14}C]torcetrapib-A to mice are shown in fig. 4. C_{max} values of torcetrapib were 2040 and 2800 ng/ml for males and females, respectively and occurred at 1 h postdose (Table 2). Terminal phase $t_{1/2}$ of torcetrapib was estimated as 1.8 and 1.3 h for males

and females, respectively. $AUC_{(0-\infty)}$ of torcetrapib was 4640 and 7760 ng·h/ml, for male and female mice, respectively (Table 2).

For total radioactivity in male mice, C_{max} of 9380 ng Eq/ml occurred at 2 h postdose (Table 3), while in females, C_{max} of 9810 ng Eq/ml occurred at 8 h postdose, which was only slightly higher than the concentration at 2 h postdose which was observed at 9610 ng Eq/ml. The terminal phase $T_{1/2}$ of total radioactivity was estimated as 11.7 and 12.2 h for males and females, respectively. $AUC_{(0-\infty)}$ of total radioactivity were 79200 ng Eq·h/ml and 110000 ng Eq·h/ml for males and females, respectively (Table 3). Based on AUC values, the majority of circulating radioactivity was attributable to metabolites.

Metabolic Profiles. Rat urine:

A representative HPLC radiochromatogram for urinary metabolites of [^{14}C]torcetrapib-A is shown in fig. 5. There were no qualitative differences in the urinary metabolic profiles between male and female rats. The mean percentages of urinary metabolites in relation to the administered dose excreted from the feces of male and female rats are presented in Table 4. A total of four radioactive peaks were observed in rat urine. These were identified as M5 (6.41 and 6.37 %); M4 (11.9 and 9.63 %)); M21 (0.94 and 1.87 %) and M22 (1.98 and 3.75 %) of the dose in male and female rats, respectively.

A representative HPLC radiochromatogram for urinary metabolites of [^{14}C]torcetrapib-B is shown in fig. 6. Five radioactive peaks were detected in rat urine. Unchanged BTFMBA accounted for 1.5% of the dose excreted in the urine. The glucuronide conjugate of BTFMBA, M26 (a-d) and M28 were the two major peaks in radiochromatogram, representing a mean 13.3 and 4.10% of the dose.

DMD Fast Forward. Published on July 24, 2008 as DOI: 10.1124/dmd.108.022277
This article has not been copyedited and formatted. The final version may differ from this version.

Rat feces. A representative HPLC radio-chromatogram for fecal metabolites of [^{14}C]torcetrapib-A in rats is shown in fig, 5. Mean percentages of fecal metabolites in relation to the administered dose excreted from the feces of male and female rats are shown in Table 4. A total of 5 radioactive peaks were observed in rat fecal samples. The unchanged torcetrapib constituted the major peak in the radiochromatogram and accounted for 33.6 and 39.3% of the dose in male and female rats, respectively. Other metabolites identified were, M2 (0.69 and 0.63%), M7 (6.5 and 7.12%), M12 (4.82 and 3.60), and M13 (6.75 and 2.03 %) of the dose in male and female rats, respectively.

Rat Bile. A representative radiochromatogram of biliary metabolites of [^{14}C]torcetrapib-A in rats is shown in fig. 7. Mean percentage of biliary metabolites of in relation to total radioactivity excreted in bile of male and female rats is shown in Table 5. Several peaks were detected in the radiochromatogram of bile from rats. There were no qualitative differences in the biliary metabolic profile of the male and female rats. Approximately 82 and 89% of the radioactivity excreted in bile was identified in males and females, respectively. The remaining radioactivity could not be distinguished from the background. The metabolites identified in the bile of rats were the glucuronide conjugate of quinoline 2-carboxylic acid, M5 (13.5%), quinoline-2-carboxylic acid, M4 (13.6%), glucuronide conjugate of hydroxylated M2 (M8A, 7.9%), M8B (6.1%), M7 (30.1%) and M13 (14.0%).

Rat plasma. A HPLC radiochromatogram of circulating metabolites at 4 h postdose of rats dosed with [^{14}C]torcetrapib-A is shown in fig. 7. The relative percentage of metabolites in relation to total circulating radioactivity at 4 h and 6 h postdose is listed in Table 6. Four radioactive peaks were observed in plasma samples from rats. Three peaks were identified as unchanged torcetrapib, M3 and M4. These peaks accounted for 30.1, 24.1 and 31.8% of the

circulating radioactivity at 4 h and 38.0, 17.7, 37.5% of the circulating radioactivity at 6 h after dosing, respectively. The fourth peak eluting at approx. 29 min was not identified due to lack of sample.

The HPLC radiochromatogram of circulating metabolites at 6 h postdose of rats dosed with [^{14}C]torcetrapib-B is shown in fig. 6. Unchanged torcetrapib and metabolite M1 were the only two peaks that were observed in plasma sample.

Monkey urine. A representative HPLC radiochromatogram for urinary metabolites of [^{14}C]torcetrapib-A in monkeys is shown in fig. 8. The individual and mean percentages of urinary metabolites in relation to the administered dose excreted in urine of male and female monkeys are shown in Table 7. A total of five radioactive peaks were observed in the monkey urine. These were identified as M10 (9.91%), M11A (9.13%), M11B (4.32%), M16 at (3.43%) and M23 (1.65%).

Monkey feces. A representative HPLC radio-chromatogram for metabolites [^{14}C]torcetrapib-A in the monkey feces is shown in fig. 8. A total of five radioactive peaks were observed in monkey fecal samples. Mean percentage of metabolites in relation to the administered dose excreted in feces of male and female monkeys is shown in Table 7. Torcetrapib constituted the major peak in the radiochromatogram and accounted for 40% of the dose. The other metabolites were identified as M2 (1.38%), M6A (0.59%), M6B (1.23%) and M10 (0.68%).

Monkey Bile. A representative HPLC-radiochromatogram for biliary metabolites of [^{14}C]torcetrapib-A is presented in fig. 9. A total of eleven metabolites were identified in bile, however, no parent torcetrapib was detected by β-ram or LC/MS/MS. The percentage of

metabolites with respect to total administered radioactive dose is presented in Table 5. All the identified metabolites constituted <2% of the total dose, excreted in bile.

Monkey Plasma. The representative HPLC radiochromatogram for metabolites [^{14}C]torcetrapib-in plasma is shown in fig. 9. The mean percentages of circulating metabolites for male and female monkeys are shown in Table 6. Six radioactive peaks were observed in the monkey plasma. These were identified as M3 which co-eluted with M9, M8A, M8B, M10, and M11and unchanged torcetrapib. In pooled plasma from 0-8 h, the mean percentage of circulating metabolites M3+M9, M8, M10, M11 and torcetrapib was 28.0, 24.2, 15.1, 10.7 and 11.3% of the total circulating radioactivity, respectively. In pooled plasma from 12-24 h, the mean percentage of circulating metabolites M3+M9, M8, M10, M11 and CP-529,414 was 38.3, 16.9, 22.1 8.0 and 14.8% of the total circulating radioactivity, respectively.

Mouse urine. A Representative HPLC-radiochromatogram of urinary metabolites of [^{14}C]torcetrapib-A in mice is shown in fig. 10. A total of 6 radioactive peaks were detected in the chromatogram. Mean percentage of metabolites in relation to the administered dose excreted in feces of male and female mice is shown in Table 8. The metabolites were identified as M3 (3.05%), M4 (5.0%), M17 (1.4%), M20 (8.9%), M21 (8.3%) and M22 (3.3%).

Mouse Feces. A representative HPLC-radiochromatogram of fecal metabolites of [^{14}C]torcetrapib-A in mice is shown in fig. 10. Torcetrapib and a total of 3 metabolites were detected. Mean percentages of metabolites in relation to the administered dose excreted in feces of male and female mice are shown in Table 8. Torcetrapib constituted the major peak in the radiochromatogram and accounted for 33.9% of the dose. The other metabolites were identified as M2 (1.8%), M6 (2%), and M13 (4.15%)

Mouse plasma. A representative HPLC-radiochromatogram of circulating metabolites of [^{14}C]torcetrapib-A at 2 h postdose from male mice is shown in fig. 10. A total of 4 radioactive peaks were detected in the chromatogram. The mean percentages of circulating metabolites for male and female mice are shown in Table 6. The metabolites were identified as unchanged torcetrapib (6.83 and 11.7%), M2 (3.71 and 3.88%), M4 (41.8 and 25.0%) and M11 (40.2 and 47.2%) of the circulating radioactivity in male and female mice, respectively.

Mass Spectral Fragmentation of Torcetrapib

Torcetrapib had a retention time of ~ 40 min on the HPLC system. Full scan MS of torcetrapib produced an intense ion at *m/z* 618 [M+NH_4^+]. The product ion mass spectrum of *m/z* 618 gave major fragment ions at *m/z* 300, 272, 254 and 228 as shown in fig. 11. The major fragment ion at *m/z* 300 resulted from the loss of the N-(bis-trifluoromethylbenzyl)methylcarbamate moiety from torcetrapib. The fragment ions at *m/z* 272 and 254 resulted from loss of the ethylene group and an ethanol moiety, respectively from *m/z* 300. The ion at *m/z* 228 resulted from loss of the ethylcarbamoyloxy group from *m/z* 300.

Identification of Metabolites. The structures of metabolites were elucidated by ion spray LC/MS/MS using combination of Q1, product ion and MRM scanning and accurate mass determination techniques (Kamel and Prakash, 2006; Prakash et al., 2007)**.**

Metabolite M1. Metabolite M1 was detected in the urine, bile, plasma and feces of rats dosed with [^{14}C]torcetrapib-B. It gave a signal at *m/z* 257 in the negative ion mode. The product ion mass spectrum of *m/z* 257 gave a major fragment ion at *m/z* 213, which was attributed to the loss of the carboxyl group. The mass spectrum and retention time of peak was similar that of the synthetic standard of BTFMBA

DMD Fast Forward. Published on July 24, 2008 as DOI: 10.1124/dmd.108.022277
This article has not been copyedited and formatted. The final version may differ from this version.

Metabolite M2. Metabolite M2 was detected in all species dosed with [^{14}C]torcetrapib-A. M2 showed a protonated molecule of *m/z* 529, 72 Da lower than the parent compound, suggesting a loss of the methyl *N*-bis-trifluoromethylbenzyl carbamate moiety. The accurate mass (observed 529.1560 vs calculated mass of 529.1538, Δ4.2 ppm error) of M2 suggested its empirical formula as $C_{23}H_{22}N_2O_2F_9$. The CID spectrum of M2 (*m/z* 529) produced a major fragment ion at *m/z* 228, same as the parent compound. The mass spectrum and the HPLC retention time of M2 was similar to those of a synthetic standard (methyl 3,5-bis(trfluoromethyl)benzyl-(2-ethyl-6-(trifluoromethyl)-1,2,3,4-tetrahydroquinoline-4-yl)carbamate.

Metabolite M3. Metabolite M3 (*m/z* 212) was detected in mouse urine and rat and monkey plasma. M3 displayed a protonated molecule of *m/z* 212, lower than the parent compound, suggesting that it was a cleaved product of torcetrapib. Accurate mass analysis of protonated ion was determined to be 212.0701 (Δ 1.0 ppm, theoretical), corresponding to an empirical formula of $C_{11}H_9NF_3$. The CID spectrum of M3 gave minor fragment ions at *m/z* 196, 192, and 143 (Fig. 12). Comparison of the spectrum and retention time of M3 with that of the synthetic standard suggested that M3 was 2-methyl-6-trifluoromethylquinoline.

Metabolite M4. Metabolite M4 was detected in rats and mice. M4 displayed a protonated molecule of *m/z* 242, lower than the parent compound, suggesting that it was also a cleaved product of torcetrapib. Accurate mass analysis of protonated ion was determined to be 242.0429 (Δ 1.8 ppm, theoretical), corresponding to an empirical formula of $C_{11}H_7NO_2F_3$. The CID spectrum of M4 at *m/z* 242 gave fragment ions at *m/z* 214, 196 and 176. The ion at *m/z* 196 loss of the formic acid (46 Da) from *m/z* 242, suggested the presence of a carboxylic acid (Fig. 12). ^{1}H NMR of M4 contained only five resonances in the entire spectrum representing five protons in two distinct spin systems (Fig. 13). Three of the five aromatic resonances (8.49,s; 8.35,d, and

8.12,d) were consistent with the presence of the phenyl ring containing one trifluoromethyl group. The two remaining aromatic resonances (8.80, d and 8.30, d) were consistent with the formation of a new aromatic ring. The lack of any other resonance indicated that the bistrifluoromethyl ring, the ethoxy, ethyl, piperidine and carbamate moieties were missing. Based on these data, M4 was identified as the quinoline-2-carboxylic acid. The structure was further confirmed by comparison of its HPLC retention time and CID spectrum with those of a synthetic standard.

Metabolites M5: Metabolites M5 was detected only in rat urine and bile as a mixture of four isomers. All four isomers displayed a protonated molecule of *m/z* 418, 176 Da higher than the metabolite M4, suggesting that all metabolites were glucuronide conjugates of M4 and that the four peaks resulted from the acyl-rearrangement of the glucuronide conjugate. The CID spectra of all the four isomers were very similar. The representative spectrum of M5 at *m/z* 418 resulted in fragment ions at *m/z* 400, 242, 196. The fragment ion at *m/z* 242 was similar to the molecular ion of quinoline-2-carboxylic acid M4 and the ion at *m/z* 196 was a result of the loss of the carboxyl group from M4.

Metabolite M6. Metabolite M6 was found only in mouse and monkey feces. M6 displayed a protonated molecular ion at m/z 545, 16 Da higher than the metabolite M2 suggesting it was a hydroxylated metabolite of M2. The exact mass of M6 was determined as 545.1453, corresponding to an empirical formula of $C_{23}H_{22}N_2O_3F_9$ (Δ -6.3 ppm, theoretical). The CID product ion spectrum of M6 gave only one ion at m/z 244. Based on the empirical formula and CID spectrum, M6 was identified as a hydroxy metabolite of M2.

Metabolite M7. Metabolite M7 was only detected in the rat feces and bile. M7 displayed a protonated molecule of *m/z* 559, 30 Da higher than the metabolite M2, suggesting the oxidation

of the methyl group to a carboxylic acid. The CID spectrum of M7 at *m/z* 559.gave major fragment ions at *m/z* 258 and 198, which were resulted from the loss of the methyl N-bis-trifluoromethylbenzyl carbamate moiety and a subsequent loss of acetic acid. Based on these data, M7 was identified as methyl 3,5-bis(trifluoromethyl)benzyl(2-carboxyethyl-6-(trifluoromethyl)-1,2,3,4-tetrahydroquinolin-4-yl)carbamate.

Metabolites M8A and M8B. Metabolites M8A and M8B were found only in bile of rats. Both M8A and M8B displayed a protonated molecule of *m/z* 721, 192 Da higher than the metabolite M2, suggesting that they both were glucuronide conjugates of the hydroxylated metabolites of M2. A representative CID spectrum of M8 at *m/z* 721 gave two fragment ions at *m/z* 420 and 244. The major fragment ion at *m/z* 420 indicated a loss of the bis-trifluoromethylbenzyl amine moiety and the ion at *m/z* 244 indicated a loss of 176 Da from ion at *m/z* 420. The exact positions of the hydroxy groups could not be determined from the mass spectra.

Metabolite M9. M9 was found only in monkey bile and plasma. M9 displayed a protonated molecule of *m/z* 242, lower than the parent compound, suggesting that it was a cleaved product of torcetrapib. Accurate mass analysis of protonated ion was determined to be 242.0793 (Δ 1.0 ppm, theoretical), corresponding to an empirical formula of $C_{12}H_{11}NOF_3$. (Δ 1.0 ppm, theoretical). The CID spectrum of M9 gave fragment ions at *m/z* 224, 196, 186 and 170. The fragment ion at *m/z* 224 indicated a loss of water molecule suggesting that the ethyl side chain was hydroxylated. The fragment ion at *m/z* 196 was a result of the loss of ethylene moiety from *m/z* 224. Based on these data, M9 was tentatively identified as the 2-hydroxyethyl-6-trifluoromethylquinoline. The exact location of hydroxyl group in M9 could not be ascertained from this data.

Metabolite M10. Metabolite M10 was detected only in monkeys. M10 displayed a protonated molecular ion at *m/z* 322.0367 in full scan MS. Elemental analysis of this data gave a molecular formula $C_{12}H_{11}NO_4F_3S$, indicating a sulfate conjugation of metabolite M9. The CID spectrum of M10 gave fragment ions at *m/z* 242 and 224. The fragment ion at *m/z* 242 suggested a loss of 80 Da from the molecule and the fragment ion at *m/z* 224 indicated a loss of 98 Da from ion at *m/z* 322. Based on these data, M10 was tentatively identified as a sulfate conjugate of hydroxyethyl-6-trifluoromethylquinoline (M9).

Metabolites M11A and B. Metabolites M11A and B were detected in bile and plasma of monkeys.. Both metabolites displayed a protonated molecule of *m/z* 418, 176 Da higher than the metabolite M4 or M9, suggesting that both metabolites were glucuronide conjugates of M4 and/or M9. The CID spectra of M11A and M11B were identical and showed major fragment ions at *m/z* 242 and 224. The accurate mass of the fragment ion at *m/z* 242 was similar to metabolite M9. These data suggested that both the metabolites were glucuronide conjugates of hydroxethyl-6-trifluoromethylquinoline (M9).

Metabolites M12. Metabolite M12 was detected only in rat feces and bile. M12 showed a protonated molecule of *m/z* 617, 16 Da higher than the parent compound. The CID product ion spectrum at *m/z* 617 showed fragment ions at *m/z* 316 and 270. The ion at *m/z* 617 suggested hydroxylation of torcetrapib. The fragment ions at *m/z* 316 and 270 resulted from loss of the methyl N-bis-trifluoromethylbenzyl carbamate moiety and subsequent loss of ethanol. The position of the hydroxy group could not be determined from the mass spectrum.

Metabolites M13. Metabolite M13 was detected in both rat and mouse. M13 showed a protonated molecular ion at *m/z* 631.1516 (30 Da higher than the parent drug). Elemental analysis of this data gave a molecular formula $C_{26}H_{24}N_2O_6F_9$ (Δ 3.9 ppm, theoretical), suggesting

the oxidation of the methyl group to a carboxylic acid. M13 showed prominent fragment ions at *m/z* 330, 270 and 198. The fragment ions at *m/z* 330 and 270 resulted from loss of the methyl N-bis-trifluoromethylbenzyl carbamate moiety and subsequent loss of an acetic acid. The minor fragment ion at *m/z* 198 resulted from loss of the ethylcarbamoyloxy group from *m/z* 270. Based on these data, M13 was identified as. 4-[*bis*-trifluoromethylbenzyl)-methoxycarbonyl-amino]-2-carboxyethyl-6-trifluoromethyl-3,4-dihydro-2H-quinoline-1-carboxylic acid ethyl ester.

Metabolite M15. Metabolite M15 was detected only in monkey bile. M15 displayed a protonated molecular ion at *m/z* 258, 16 Da higher than M4 and M9, suggesting that it was a hydroxylated metabolite of either M4 or M9. Accurate mass determination provided molecular formula to be equivalent to $C_{12}H_{11}NO_2F_3$. CID product ion spectrum of M15 produced fragment ions at *m/z* 240, 212, 211 and 143. Based on this information, M15 was tentatively identified as hydroxyl trifluoromethyquinolinylethanol**.**

Metabolite M16. Metabolite M16 was detected only in monkey urine. M16 displayed a protonated molecular ion at *m/z* 434, 176 Da higher than M15, suggesting that it was a glucuronide conjugate of M15. Based on these data, M16 was identified as a glucuronide conjugate of hydroxy-trifluoromethyquinolinylethanol (M15).

Metabolite M17. Metabolite M17 was found only in mouse urine and plasma. M17 showed a protonated molecular ion at *m/z* 228. Accurate mass analysis of protonated ion was determined to be 228.0636, corresponding to an empirical formula of $C_{11}H_9NOF_3$ (Δ 0.1 ppm, theoretical). The CID spectrum of M17 showed prominent fragment ions at m/z 210.0554 and 190.0489 (Fig. 14). Comparison of the CID spectrum and retention time of M17 with those of the synthetic standard suggested that M17 was 6-trifluoromethylquinolin-yl-methanol.

Metabolite M18. Metabolite M18 was detected only in monkey bile. Its full scan MS displayed a protonated molecular ion at *m/z* 659. The CID product ion spectrum of *m/z* 659 gave major fragment ions at *m/z* 483 and 465 and minor fragment ions at *m/z* 238, 141 and 113. Fragment ion at *m/z* 483 was due to loss of the glucuronide from the parent ion, and additional loss of a water molecule gave fragment ion at *m/z* 465. Fragment ion at *m/z* 238 resulted by cleavage of the bis-trifluoromethybenzyl moiety and subsequent losses of the glucuronide and water at the trifluoromethyl quinoline portion of the molecule. Additionally, accurate mass measurements of M18 gave an elemental composition of $C_{27}H_{24}N_2O_7F_9$. Based on these data, M18 was tentatively identified as a glucuronide conjugate of 4-(3,5-bis-trifluoromethyl-benzylamino)-2-hydroxyethyl-6-trifluoromethyl-quinoline.

Metabolite M19. Metabolite M19 was detected in monkey bile. Its full scan MS showed a protonated molecular ion at *m/z* 717. The CID product ion spectrum of *m/z* 717 gave fragment ions at *m/z* 541, 523, 283, 254 and 227. Fragment ion at *m/z* 541, loss of 176 Da from the parent ion, suggested that it was a glucuronide conjugate. Fragment ion at *m/z* 523 was due to the subsequent loss of a water molecule from ion at *m/z* 541. Product ion at *m/z* 283 resulted by cleavage of the bis-trifluoromethybenzyl moiety and subsequent losses of the glucuronide and CH_3O (31 Da) and ion at *m/z* 265 was an additional loss of water from ion at *m/z* 283. The

accurate mass measurements of M19 gave an elemental composition of $C_{29}H_{26}N_2O_9F_9$. Based on this data, M19 was tentatively identified as a glucuronide conjugate of 4-(3,5-bis-trifluoromethyl-benzyl-methoxycarbonyl-amino)-2-hydroxyethyl-6-trifluoromethyl-quinoline.

Metabolite M20. Metabolite M20 was found only in mouse urine. M20 showed a protonated molecular ion at *m/z* 349, 107 Da higher than M4, suggested conjugation of M4 with taurine. The accurate mass of MH^+ (349.0471) proposed the empirical formula of $C_{13}H_{12}N_2O_4F_3S$ (Δ 0.2 ppm, theoretical). MS/MS spectrum of M20 showed prominent fragment ions at *m/z* 331, 242, 224, 214 and 196. Based on this data, M20 was tentatively identified as the taurine conjugate of M4.

Metabolite M21. Metabolite M21 was found in mouse urine. Its protonated molecular ion at m/z 299, 57 Da higher than the metabolite M4, suggesting that M21 was a glycine conjugate of M4. The accurate mass of MH^+ (299.0636) proposed the empirical formula of $C_{13}H_{10}N_2O_3F_3$ (Δ -2.6 ppm, theoretical). MS/MS spectrum of M21 showed prominent fragments at m/z 253, 224, 214 and 196. The fragment ions at *m/z* 253 and 224 resulted from loss of the formic acid and glycine moiety from *m/z* 299, respectively. The ion at *m/z* 196 was characteristic of the quinoline-2-carboxylic acid (M4). Based on these data, the structure of M21 was identified as glycine conjugate of M4.

Metabolite M22. Metabolite M22 was found only in mouse urine. It displayed a protonated molecular ion at *m/z* 284, 42 Da higher than the metabolite M4, suggesting that M21 was a conjugate of M4. The accurate mass of MH^+ (284.0652) proposed the empirical formula of $C_{12}H_9N_3O_2F_3$ (Δ -0.2 ppm, theoretical), which corresponded to a urea conjugate of M4. MS/MS spectrum of M22 gave prominent fragments at *m/z* 224, 214 and 196 (Fig. 14). M22 rapidly

DMD Fast Forward. Published on July 24, 2008 as DOI: 10.1124/dmd.108.022277
This article has not been copyedited and formatted. The final version may differ from this version.

loses NH_3 in the ion source to form an ion at *m/z* 267, with an empirical formula of $C_{12}H_4N_2O_2F_3$. The other fragment ions at *m/z* 224 resulted from loss of the urea moiety from *m/z* 299. Based on these data, M22 was identified as the urea conjugate of M4.

Metabolite M26. Metabolite M26 was detected in the urine of rats dosed with [^{14}C]torcetrapib-B as a mixture of four isomers. All four isomers displayed a deprotonated molecule $[M-H]^-$ of *m/z* 433 in the negative ion mode, 176 Da higher than the BTFMBA, suggesting that all metabolites were glucuronide conjugates of BTFMBA and that the four peaks resulted from the acyl-rearrangement of the glucuronide conjugate. The product ion mass spectrum of *m/z* 433 gave major fragment ions at *m/z* 257, 175 and 113. The fragment ions at *m/z* 257 and 175 were characteristic of BTFMBA (M1) and the glucuronic acid moiety, respectively. Furthermore, the metabolite was readily hydrolyzed by sodium hydroxide. Based on this data M26 was identified as the glucuronide conjugate of M1.

Metabolite M27. Metabolite M27 was detected in the urine of rats dosed with [^{14}C]torcetrapib-B. It gave a signal at *m/z* 419 in the negative ion mode. Hydrolysis of M27 by ß-glucuronidase gave a product that co-eluted with synthetic bis-trifluoromethylbenzyl alcohol. Thus M27 was tentatively identified as the glucuronide conjugate of 2,5-bistrifluorobenzylalcohol.

Metabolite M28. Metabolite M28 was detected in the urine of rats dosed with [^{14}C]torcetrapib C-14 labeled at the benzylic position. M28 displayed a deprotonated molecule $[M-H]^-$ of *m/z* 380 in the negative ion mode. The product ion mass spectrum of *m/z* 380 gave a major fragment ion at *m/z* 81, which was attributed to the sulfonate moiety and minor fragment ions at *m/z* 348, 284 and 240. The fragment ion at *m/z* 348 and 284 indicated a loss of the methanol moiety and a sulfonate moiety from *m/z* 380 and the ion at *m/z* 240 suggested the loss of the methylcarbamoyloxy and sulfonate moieties from *m/z* 380. These data suggested that the

metabolite was bisulfite adduct of methyl carbamate. The high-resolution mass spectrum of M28 suggested the empirical formula of $C_{11}H_9F_6NO_5S$. ^{1}H NMR of M28 contained two aromatic resonances (3H total), suggesting that bis(trifluoromethyl)phenyl ring was unsubstituted. The methyl resonance at δ 3.61 ppm was indicative of no change to the methyl carbamate moiety; the methine proton at δ 5.70 ppm was indicative of the sulfite substitution at the benzylic position (Fig. 15). Based on these data, M28 was identified as 3,5 bis(trifluoromethyl)phenyl)-(methoxycarbony-aminol)methanesulfonic acid. The structure of M28 was consistent with HMBC correlations and was unequivocally confirmed by comparison of its HPLC retention time and mass spectrum with those of the synthetic standard.

Discussion

We here report the metabolic fate and disposition of torcetrapib in rats, monkeys and mice, the animal species used for safety toxicology and carcinogenicity studies. [^{14}C]torcetrapib, labeled at the trifluoromethyl-3,4-dihydro-2H-quinoline moiety, was administered orally to rats, monkeys and mice. Additionally, [^{14}C]torcetrapib labeled at the benzylic carbon of the bis-trifluorophenyl ring was administered to SD rats to determine the fate of bis-trifluoromethylbenzoic acid formed by N-dealkylation of the tetrahydroquinoline moiety of torcetrapib. The use of C-14 label at two different positions not only facilitated the tracing of metabolites that were formed through oxidative cleavage of torcetrapib but also aided in their identification. The administered radioactive dose was quantitatively recovered in all species (rat, 93.4/94.4%; monkey, 86.8% and mouse 90.7%). Excretion of the radioactivity was rapid and nearly complete within 48 h after dosing. In the rats and monkeys, the majority of dose was excreted in feces while in the mice, the dose was recovered equally in urine and feces. In the

separate studies using bile-duct cannulated rats and monkeys, <10% % of the administered radioactivity was recovered in bile. This suggested that a major portion of dose excreted in the feces of rats and monkeys was mainly due to unabsorbed dose. There were no discernible gender differences in the excretion pattern of radioactivity in these species after oral administration of [^{14}C]torcetrapib-A. However, pharmacokinetics of torcetrapib and total radioactivity displayed distinct gender-related differences in male and female rats and mice but not in monkeys. The exposure (C_{max} and AUC) of torcetrapib and total radioactivity was higher in females compared to males. In addition, the $t_{1/2}$ values of total radioactivity and unchanged torcetrapib were similar in monkeys but the $t_{1/2}$ of total radioactivity was 2.7 and 8 fold greater than the $t_{1/2}$ of the parent compound in rats and mice, respectively, suggesting that one or more of the metabolites circulated for a longer time in these species. The gender-related differences in the pharmacokinetics of xenobiotics, especially for rats, have been well known and can be result of the differences in hormone levels, plasma protein binding, and/or expression level of drug metabolizing enzymes (Tanaka et al., 1991a, 1991b; Prakash and Soliman, 1997).

The urine and/or bile radiochromatograms from rats, monkeys and mice indicate that torcetrapib is extensively metabolized before excretion since no unchanged drug was detected in urine or bile. The major portion of administered radioactivity was excreted in urine and bile as the products of oxidation and conjugation pathways. There were no gender- related qualitative differences in the profile of metabolites. However, there were notable species related qualitative and quantitative differences in the metabolic profiles. More than twenty eight metabolites were identified in all species by ion spray LC/MS/MS (Kamel and Prakash, 2006; Prakash et al., 2007). A proposed scheme for the biotransformation pathways of torcetrapib in rats, monkeys and mice is shown in fig 16. The primary metabolic pathway in all species involved hydrolysis

DMD Fast Forward. Published on July 24, 2008 as DOI: 10.1124/dmd.108.022277
This article has not been copyedited and formatted. The final version may differ from this version.

of the ethyl carbamate moiety to form metabolite M2, which then underwent oxidation at the ethyl group with subsequent glucuronidation, and/or aromatization of the tetrahydroquinoline moiety. The other major metabolites were due to multiple oxidation and conjugation of the trifluoromethyl-3,4-dihydro-2H-quinoline moiety.

The major circulating and excretory metabolites in rats, monkeys, and mice were species-dependent; however, several common metabolites were observed in more than one species (e.g., M1, M3, M4, M8A, M8B, M11 and M13). The major components of drug related material in rat excreta were identified as M4 (10.8%), M5 (6.39%), M7 (6.81%), M12 (4.1%) and M13 (4.39%). The metabolic profile in male and female rats was qualitatively similar. However, the metabolite M13, the acid derivative of torcetrapib was 3 fold higher in the feces of male rats than that of females. Two major circulating metabolites, M3 and M4 were detected at 4 and 6 h post dose, in the male and female rats. The percentage of the circulating metabolite M4 was similar to that of parent at both time points whereas the M3/torcetrapib ratio was 0.8 and 0.46 at 4 and 6 h postdose, respectively. Studies with [^{14}C]torcetrapib, with the label at the benzylic position, indicated that BTFMBA (M1) was the major metabolite in rats and accounted for 94% of the circulating radioactivity although only 3.5% of the total dose was excreted as M1. Glucuronidation was the primary route of clearance of M1 and represented 13.3% of the total dose in rats. In addition, an unusual and novel metabolite, a bisulfite adduct of methyl carbamate (M28), was also detected in the urine and accounted for 8.67 % of the total dose.

The major oxidative metabolites in monkeys were due to multiple oxidations to form 2-hydroxyethyl-6-trifluoromethylquinoline metabolite (M9). It was further metabolized to form major metabolites M10, (sulfate conjugate), M11 (glucuronide conjugate) and M16 (a

glucuronide conjugate of its hydroxyl metabolite (M15). The metabolite M10, the sulfate conjugate was 3.5 fold higher in the excreta of male rats than that of females. Two major circulating metabolites were identified as M8, M9 and M10 in both male and female monkeys.

In addition to unchanged torcetrapib, a total of nine metabolites were identified in mice. Of all drug-related materials, unchanged torcetrapib in feces comprised the greatest abundance at 36.3 and 31.4% of dose in males and females, respectively. Metabolites M20 (taurine conjugate) and M21 (glycine conjugate), both in urine, were present at 8.9 and 8.3% of the dose respectively. All other excretory metabolites were present at less than 6% of dose, and included M2, M3, M4, M6, M13, M17, and M22. The major circulating metabolites in mice include M4 and M11 which ranged from 25 to 47% of total radioactivity. Torcetrapib comprised 6.8 and 11.7% of radioactivity in males and females, respectively.

In this study, several novel and unusual quinoline metabolites (M3, M4, M5, M9, M17, M22) and a sulfite conjugate M28, formed by multiple pathways (N-dealkylation, oxidation, aromatization, and sulfation), were identified. The structures of two metabolites M4 and M28 were elucidated by accurate mass measurements and LC-NMR. M4 was detected only in rats dosed with [^{14}C]torcetrapib labeled at the tetrahydroquinoline ring, suggesting loss of the *bis*-(trifluoromethyl)phenyl ring of torcetrapib. One of the spin systems (two doublets coupled to each other and a singlet) in the ^{1}H NMR of M4 were consistent with the presence of the phenyl ring containing one trifluoromethyl group. The other spin system (two doublets coupled to each other) indicated the aromatization of the tetrahydroquinoline of torcetrapib. The aromatization of the N-substituted tetrahydroquinoline and tetrahydropyridines has been reported and catalyzed by several P-450s, MAOs, horseradish peroxidase and myloperoxidase (Shaffer et al.,

2001; Dalvie and O'Connell, 2004; Obach and Dalvie, 2006; Gu et al., 2006). The mechanism and the enzyme(s) involved for the formation of M4 are not known at this time.

On the other hand, sulfonic acid conjugate metabolite M28 was detected only in rats dosed with [^{14}C]torcetrapib labeled at the benzylic carbon of the bis-trifluoromethylphenyl ring, suggesting loss of the tetrahydroquinoline ring of torcetrapib. The presence of proton resonances at δ 8.08 ppm (2H) and 7.93 ppm (1H) in the ^{1}H NMR spectrum of M28 were consistent with the aromatic ring that contains two trifluromethyl groups. The methine resonance at δ 5.70 ppm suggested that the substitution of a sulfonate group had occurred at the benzylic position. The proton resonance at δ 3.61 ppm (3H) and its corresponding carbon resonance at 54 ppm were consistent with the methyl group of the carbamate moiety. The mechanism for the formation of M28 is under investigation and will be reported separately. These types of sulfonic acid metabolites are rare but have been reported, and are formed by either degradation of cysteine and glutathione conjugates or direct addition of sulfite ion (Yoshino et al., 1993; He et al., 2003; Chen et al., 2003).. Therefore, the formation of M28 can be speculated by initial formation of the methyl bis(trifluoromethyl)-benzylidenecarbamate followed by conjugation with glutathione, subsequent cleavage of the C-S bond (catalyzed by C-S lyase) and oxidation of SH to sulfite as reported by Yoshino et al (1993) (Fig. 17). The similar electrophilic metabolite and GSH conjugate of capsaicin have been reported in laboratory animals (Reilly and. Yost, 2006).

In summary, torcetrapib was primarily cleared by metabolism in the nonclinical species. The primary metabolic pathway of torcetrapib involved hydrolysis of the carbamate ester (M2) and the oxidation of the ethyl moieties. M2 was further metabolized by oxidative cleavage to novel

and unusual quinoline metabolites and 3, 5-bistrifluoromethyl benzoic acid (M1). The major circulating and excretory metabolites in mice, rats and monkeys were species-dependent, however, several common metabolites were observed in more than one species.

Acknowledgments. We would like to thank Drs. Klaas Schildknegt, Roger Ruggeri and Gregory Dolnikowski for providing radiolabelled torcetrapib and synthetic metabolite standards, Jian Lin and Ms. Beth Obach for technical assistance and Drs. David Plowchalk and Scott Obach for helpful discussions.

References

Barter, P., J. Kastelein, A. Nunn, R. Hobbs, and Future Forum Editorial Board. 2003. High density lipoproteins (HDLs) and atherosclerosis: the unanswered questions. *Atherosclerosis.* **168:** 195–211.

Bruce C, Chouinard RA, Tall AR. Plasma lipid transfer proteins, high-density lipoproteins, and reverse cholesterol transport. *Annu Rev Nutr,***18**: 297-330.

Chen L-J, Lebketkin EH and Burka LT (2003) Metabolism of (R)-(+) menthofuran in fischer-344 rats:identification of sulfonic acid metabolites. *Drug Metab Dispos*. **31 (10):** 1208-1213.

Clark RW, Ruggeri RB, Cunningham D, and Bamberger MJ. (2006) Description of the torcetrapib series of cholesteryl ester transfer protein inhibitors, including mechanism of action.. *J Lipid Res*, **47(3):** 537-552.

Dalvie DK and O'Connell TN (2004) Characterization of novel dihydrothienopyridinium and thienopyridinium metabolites of ticlopidine in vitro: role of peroxidases, cytochromes P450 and monoamine oxidase. *Drug Metab Dispos* **32**: 49–57

Damon DB, Dugger RW, Magnus-Aryitey G, Ruggeri RB, Wester RT, Tu M, Abramov Y. (2006) Synthesis of the CETR inhibitor torcetrapib: The resolution route and origin of stereoselectivity in the iminium ion cyclization. *Org Proc Res Develop*, **10(3**): 464-471.

Downs JR, Clearfield M, Weis S, Whitney E, Shapiro DR, Beere PA, Langendorfer A, Stein EA, Kruyer W, Gotto AM (1998). Primary prevention of acute coronary events with lovastatin in men and women with average cholesterol levels: results of AFCAPS/Texcaps. air force/Texas coronary atherosclerosis prevention study. *JAMA*, **279**: 1615-22.

Evans GF, Bensch WR, Apelgren LD. (1994) Inhibition of cholesteryl ester transfer protein in normocholesterolemic and hypercholesterolemic hamsters: effects on HDL subspecies, quantity, and apoprotein distribution. *J Lipid Res*, **35**: 1634-5.

Food and Drug Administration (2008) Guidance for Industry: Safety Testing of Drug Metabolites. http//www.fda.gov/cder/guidance/index.htm (February 14, 2008)

Gaynor BJ, Sand T, Clark RW. (1994). Inhibition of cholesteryl ester transfer protein in hamsters alters HDL lipid composition. *Atherosclerosis*, **110**: 101-9.

Gu C, Collins R, Holsworth DD, Walker GS and Voorman RL (2006) Metabolic aromatization of *N*-Alkyl-1,2,3,4-tetrahydroquinoline substructures to quinolinium by human liver microsomes and horseradish peroxidase. *Drug Metab Dispos*, **34**: 2044-2055.

He X, Li J, Gao, H, Qiu F, Hu Ke, Cui X and Yao X (2003) Identification of a rare sulfonic acid metabolite of andrographolide in rats. *Drug Metab Dispos*. **31 (8):** 983-985.

Howes LG and Kostner K. (2007) The withdrawal of torcetrapib from drug development: implications for the future of drugs that alter HDL metabolism. *Expert Opin on Invest Drugs* **16(10):** 1509-1516.

Inazu A, Brown ML, Hesler CB (1990). Increased high density lipoprotein caused by a common cholesteryl ester transfer protein gene mutation. *N Engl J Med*, **323**: 1234-8.

Kamel A, Prakash C (2006) High performance liquid chromatography/atmospheric pressure ionization /tandem Mass spectrometry (HPLC/API/MS/MS) in drug metabolism and toxicology studies. *Curr Drug Metab*, **7**:837-852.

Marotti KR, Castle CK, Boyle TP (1993). Severe atherosclerosis in transgenic mice expressing simian cholesteryl ester transfer protein. *Nature* **364**:73-5.

Obach RS and Dalvie DK (2006) Metabolism of nomifensine to a dihydroisoquinolinium ion metabolite by human myeloperoxidase, hemoglobin, monoamine oxidase a, and cytochrome P-450 enzymes. *Drug Metab Dispos*, **34**: 1310-1316.

Plump AS, Masucci-Magoulas L, Bruce C (1999). Increased atherosclerosis in apoE and LDL receptor gene knock-out mice as a result of human cholesteryl ester transfer protein transgene expression. *Arterioscler Thromb Vasc Biol*, **19**: 1105-10.

Prakash C, Shaffer C, Nedderman A (2007) Analytical strategies for identifying drug metabolites. Mass Spectrom Rev, **26**:340-369.

Prakash C , Soliman V (1997) Metabolism and excretion of a new anxiolytic drug candidate, CP-93,393, in Long-Evans rats. *Drug Metab Dispos* **25**:1288-1297.

Reilly CA and Yost GS (2006) Metabolism of capsaicinoids by p450 enzymes:A review of recent findings on reaction mechanisms, bio-activation, and detoxification processes *Drug Metab Rev.*, **38**: 685–706

Sacks FM, Pfeffer MA, Moye LA, Rouleau JL, Rutherford JD, Cole TG, Brown L Warnica JW, Arnold JM, Wun CC, Davis BR, Braunwald E (1996)The effect of pravastatin on coronary events after myocardial infarction in patients with average cholesterol levels. *N Engl J Med,* **335:** 1001-1009.

Schaefer EJ, Brousseau ME (2000) Benefits of reducing low-density lipoprotein cholesterol concentrations to <100 mg/dL. *Prev. Cardiol*, **3:** 136-139.

Shaffer CL, Morton MD, and Hanzlik RP (2001) N-dealkylation of an N-cyclopropylamine by horseradish peroxidase: fate of the cyclopropyl group. *J Am Chem Soc,* **123**: 8502–8508
Shepherd J, Cobbe SM, Ford I, Isles CG, Lorimer AR, Macfarlane PW, McKillop JH, Packard CJ (1995) Prevention of coronary heart disease with pravastatin in men with hypercholesterolemia. *N. Engl. J. Med*, **333**: 1301-7.

Tanaka Y, Deguchi Y, Ishi I, Terai T (1991a) Sex diffrences in excretion of zenarestat in rat. Xenobiotica **21**:1119-1125.

Tanaka Y, Kadoh Y, Mukumoto S, Ishikawa H (1991b) The role of age and sex hormones on the urinary excretion of zenarestat in rats. Xenobiotica **21**:1273-1279.

Teh EM, Dolphin PJ, Breckenridge WC (1998) Human plasma CETP deficiency: identification of a novel mutation in exon 9 of the CETP gene in a Caucasian subject from North America. *J Lipid Res,* **39:** 442-6.

Whitlock ME, Swenson TL, Ramakrishman R (1989). Monoclonal antibody inhibition of cholesteryl ester transfer protein activity in the rabbit. Effects on lipoprotein composition and high density lipoprotein cholesteryl ester metabolism. *J Clin Invest*, **84**: 129-37.

Yoshino H, Matusanaga H, Kaneko H, Yoshitake A, Nakatsuka I and Yamada H (1993) Metabolism of N-[4--chloro-2-fluoro-5-[(1-methyl-2-propynyloxy]phenyl]-3,4,5,6tetrahydrophthalimide (S-23121) in the rat: identification of a new, sulfonic acid type of conjugate. *Xenobiotica*, **23**:609-619.

Footnotes:

Send reprints requests to: Chandra Prakash, Ph. D., Department of Pharmacokinetics, Dynamics and Metabolism, Pfizer Global Research and Development, Groton, CT 06340. Email:Chandra.prakash@pfizer.com

Figure Legends:

Fig. 1. Structure of [^{14}C]torcetrapib A and [^{14}C]torcetrapib-B.

Fig. 2. Mean plasma concentration-time curves of torcetrapib and total radioactivity in male and female rats oral administration a single 20 mg/kg oral dose of [^{14}C]torcetrapib-A

Fig.3. Mean plasma concentration-time curves of torcetrapib and total radioactivity in male and female monkeys oral administration a single 60 mg/kg oral dose of [^{14}C]torcetrapib-A

Fig. 4. Mean plasma concentration-time curves of torcetrapib and total radioactivity in male and female mice oral administration a single 20 mg/kg oral dose of [^{14}C]torcetrapib-A

Fig.. 5. HPLC-radiochromatograms of torcetrapib metabolites in urine and feces of rats after oral administration a single 20 mg/kg oral dose of [^{14}C]torcetrapib-A

Fig. 6. HPLC-radiochromatograms of torcetrapib metabolites in urine (A) and plasma (B) of rats after oral administration a single 20 mg/kg oral dose of [^{14}C]torcetrapib-B

Fig. 7. HPLC-radiochromatograms of torcetrapib metabolites in bile and plasma (4 h)of rats after oral administration a single 20 mg/kg oral dose of [^{14}C]torcetrapib-A

Fig. 8. HPLC-radiochromatograms of torcetrapib metabolites in urine and feces of monkeys after oral administration a single 60 mg/kg oral dose of [^{14}C]torcetrapib-A

Fig. 9. HPLC-radiochromatograms of torcetrapib metabolites in bile and plasma of monkeys after oral administration a single 60 mg/kg oral dose of [^{14}C]torcetrapib-A

Fig. 10. HPLC-radiochromatograms of torcetrapib metabolites in urine, feces and plasma (2 h) of mice after oral administration a single 20 mg/kg oral dose of [^{14}C]torcetrapib-A

Fig. 11. CID product ion mass spectrum of torcetrapib (*m/z* 618 $\{M+NH4\}^+$)

Fig. 12. CID product ion mass spectra of metabolites M3 (*m/*z 212) and M4 (*m/*z 242)

Fig. 13. ^{1}H NMR spectrum of M4 with expansion of aromatic region

Fig. 14. CID product ion mass spectra of metabolites M17 (*m/z* 228) and M22 (*m/z* 284)

Fig. 15. ^{1}H NMR spectrum of M28 and depiction of HMBC correlations

Fig. 16. Proposed biotransformation pathways of [^{14}C]torcetrapib in rats, monkeys and mice

Fig. 17. Proposed mechanism for the formation of M28

.

DMD Fast Forward. Published on July 24, 2008 as DOI: 10.1124/dmd.108.022277
This article has not been copyedited and formatted. The final version may differ from this version.

Table 1. Mean percentage dose recovered in urine and feces from rats, monkeys and mice following oral administration of [^{14}C]torcetrapib-A or [^{14}C]torcetrapib-B.

Animal	% of Dose Excreted in 0-168 h				
	Urine	Feces	Carcass	Cage Rinse	Total
Male Rats (N=3)*	21.3	59.1	7. 54	6. 87	94.8
Female Rats (N=3)*	21.6	52.7	9.87	7.74	91.9
Mean*	21.5	55.9	8.77	7.30	93.4
Male Rats (N=3)**	21.1	62.6	8.29	3.85	95.9
Female Rats (N=3)**	21.7	56.4	10.3	4.44	92.8
Mean**	21.4	59.5	9.28	4.14	94.4
Male Monkeys (N=2)*	39.0	35.1	ND	15.1	89.2
Female Monkeys (N=2)*	19.3	53.8	ND-	11.3	84.4
Mean*	29.2	44.5	ND	13.2	86.8
Male Mice (N=3/cage)*	41.2	44.3	3.05	2.51	91.1
Female Mice (N=3/cage)*	40.6	40.0	4.86	4.90	90.3
Mean*	40.9	42.1	3.96	3.71	90.7

*dosed with [^{14}C]torcetrapib-A
**dosed with [^{14}C]torcetrapib-B
ND; not determined

DMD Fast Forward. Published on July 24, 2008 as DOI: 10.1124/dmd.108.022277
This article has not been copyedited and formatted. The final version may differ from this version.

Table 2. Mean pharmacokinetic parameters for torcetrapib in rats, monkeys and mice following oral administration of [^{14}C]torcetrapib-A

Animals	T_{max} (h)	C_{max} (ng/ml)	$AUC_{(0\text{-}tlast)}$ (ng·h/ml)	$AUC_{(0\text{-}\infty)}$ (ng·h/ml)	Estimates of $T_{1/2}$ (h)
Male Rats (N=3)	2.0	1590	5800	6490	3.9
Female Rats (N=3)	3.3	2220	13400	15000	3.2
Mean	2.7	1910	9580	10800	3.5
Male Monkey (N=3)	13.0	966	40300	51300	91
Female Monkey (N=2)	6.0	783	31800	48100	112
Mean	10.4	893	36900	50000	99
Female Mice	1.0	2800	7590	7760	1.3
Male Mice	1.0	2040	4410	4640	1.8
Mean	1.0	2420	6000	6200	1.55

DMD Fast Forward. Published on July 24, 2008 as DOI: 10.1124/dmd.108.022277
This article has not been copyedited and formatted. The final version may differ from this version.

Table 3. Mean pharmacokinetic parameters for total radioactivity in rats, monkey and mice following oral administration of [^{14}C]torcetrapib-A

Animal	T_{max} (h)	C_{max} (ng Eq/ml)	$AUC_{(0\text{-}tlast)}$ (ng Eq·h/ml)	$AUC_{(0\text{-}\infty)}$ (ng Eq·h/ml)	Estmate of $T_{1/2}$ (h)
Male Rats (N=3)	6.7	3020	48300	49400	8.6
Female Rats (N=3)	5.3	4150	76900	80700	10.5
Mean	6.0	3590	62600	65100	9.6
Male Monkey (N=3)	20	7230	297000	341000	83.0
Female Monkey (N=2)	14	4620	189000	227000	76.0
Mean	17.6	6190	254000	295000	80.0
Female Mice	8.0	9810	107000	110000	12.2
Male Mice	2.0	9380	77700	79200	11.7
Mean	5.0	9600	92400	94600	12.0

DMD Fast Forward. Published on July 24, 2008 as DOI: 10.1124/dmd.108.022277
This article has not been copyedited and formatted. The final version may differ from this version.

Table 4. Relative abundance of urinary and fecal metabolites of torcetrapib in male and female rats following oral administration of [^{14}C]torcetrapib-A

Metabolites	Male Rats			Female Rats		
	Urine	Feces	Total	Urine	Feces	Total
Torcetrapib	-	33.6	33.6	-	39.3	39.3
M2	-	0.69	0.69	-	0.63	0.63
M4	11.9	-	11.9	9.63	-	9.63
M5	6.41	-	6.41	6.37	-	6.37
M7	-	6.5	6.5	-	7.12	7.12
M12	-	4.82	4.82	-	3.6	3.6
M13	-	6.75	6.75	-	2.03	2.03
M21	0.94	-	0.94	1.87	-	1.87
M22	1.98	-	1.98	3.75	--	3.75

DMD Fast Forward. Published on July 24, 2008 as DOI: 10.1124/dmd.108.022277
This article has not been copyedited and formatted. The final version may differ from this version.

Table 5. Relative abundance of biliary metabolites of torcetrapib in rats and monkeys following oral administration of [^{14}C]torcetrapib-A

	Rat Bile			Monkey Bile
Metabolite	Male	Female	Mean	Mean
M2	-	-	-	2.17
M4	10.6	16.6	13.6	-
M5	12.9	14.1	13.5	-
M6	-	-	-	2.27
M7	32.6	27.6	30.1	-
M8A	7.4	8.4	7.9	19.4
M8B	5.5	6.6	6.1	3.44
M9	-	-	-	4.94
M10	-	-	-	4.14
M11A, B	-	-	-	6.46
M13	12.8	15.2	14	-
M15	-	-	-	6.86
M18	-	-	-	8.52
M19	-	-	-	7.49

Table 6. Relative abundance of circulating metabolites of torcetrapib in rats, monkeys and mice following oral administration of [^{14}C]torcetrapib-A

	Rats		Monkeys		Mice	
Metabolites	4 HPD	6 HPD	0-8 HPD	12-24 HPD	Male	Female
M2	-	-	-	-	3.71	3.88
M4	31.8	37.5	-	-	41.8	25.0
M3	24.1	17.7	-	-	-	-
M3/M9	-	-	28.0	38.3	-	-
M8A, B	-	-	24.2	16.9	-	-
M10	-	-	26.0	22.1	-	-
M11A, B	-	-	10.7	8.0	40.2	47.2
Unknown	14.0	6.92	-	-	-	-
Torcetrapib	30.1	38	11.3	14.8	6.83	11.7

DMD Fast Forward. Published on July 24, 2008 as DOI: 10.1124/dmd.108.022277
This article has not been copyedited and formatted. The final version may differ from this version.

Table 7. Relative abundance of urinary and fecal metabolites of torcetrapib in male and female monkeys following oral administration of [^{14}C]torcetrapib-A.

Metabolites	Males			Females		
	Urine	Feces	Total	Urine	Feces	Total
Torcetrapib		30.5	30.5	-	49.5	49.5
M2		1.26	1.26	-	1.5	1.5
M6A		0.63	0.63	-	0.55	0.55
M6B		1.22	1.22	-	1.24	1.24
M16	3.88	-	3.88	2.98	-	2.98
M10	15.7	1.08	16.8	4.21	0.29	4.5
M11A	10.6	-	10.6	7.66	-	7.66
M11B	5.71	-	5.71	2.94	-	2.94
M23	2.17	-	2.17	1.12	-	1.12

Table 8. Relative abundance of urinary, and fecal metabolites of torcetrapib in male and female mice following oral administration of [^{14}C]torcetrapib-A

Metabolites	Males			Females		
	Urine	Feces	Total	Urine	Feces	Total
Torcetrapib	-	36.3	36.3	-	31.4	31.4
M2	-	1.8	1.8	-	1.8	1.8
M3	3.5	-	3.5	2.6	-	2.6
M4	5.2	-	5.2	4.8	-	4.8
M6A, B	-	1.7	1.7	-	2.3	2.3
M13	-	2.6	2.6	-	5.7	5.7
M17	1.8	-	1.8	1.0	-	1.0
M20	7.3	-	7.3	10.5	-	10.5
M21	9.6	-	9.6	7.0	-	7
M22	3.4	-	3.4	3.2	-	3.2

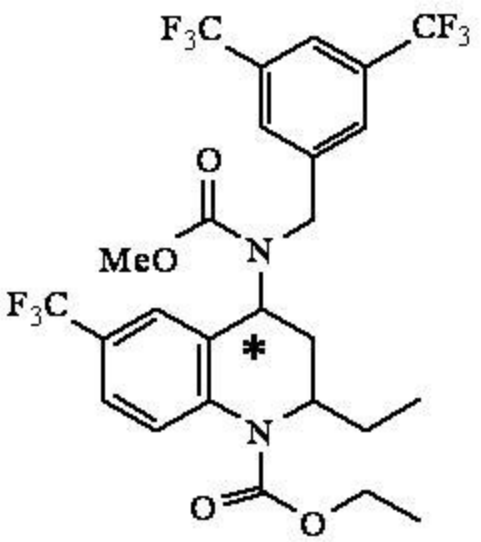

Torcetrapib-A

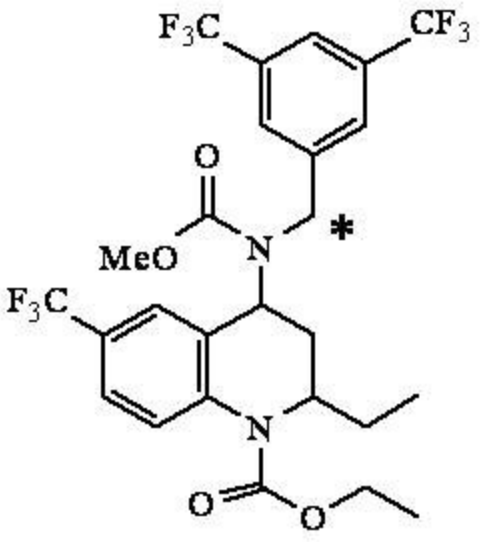

Torcetrapib-B

*Denotes sites of ^{14}C-label

Fig. 1

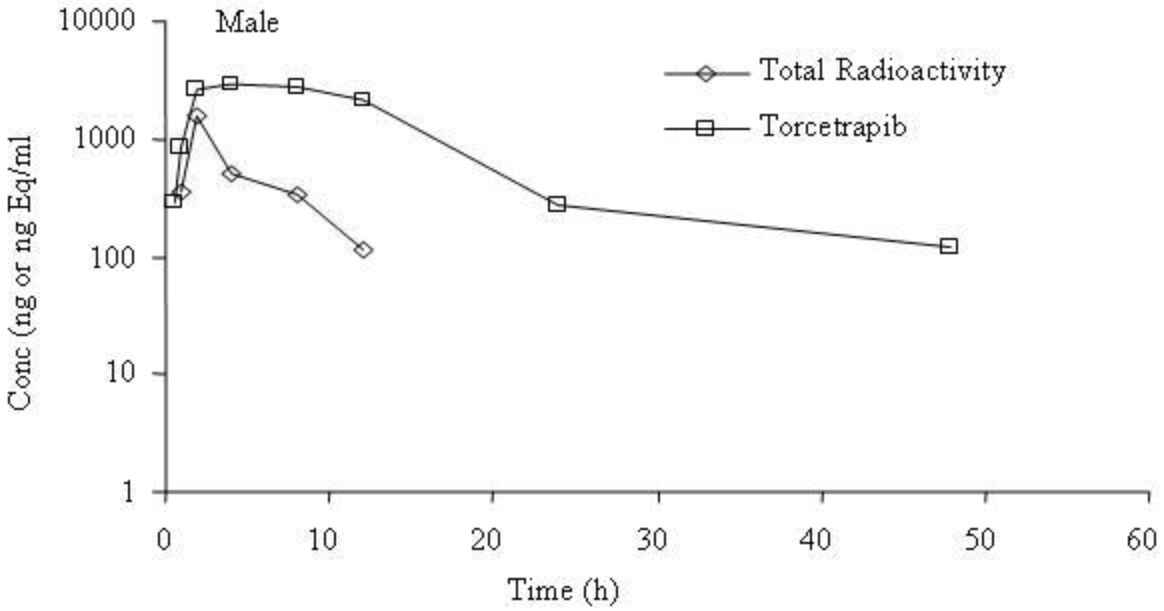
Male
Total Radioactivity
Torcetrapib
Conc (ng or ng Eq/ml
10000
1000
100
10
1
0
10
20
30
40
50
60
Time (h)

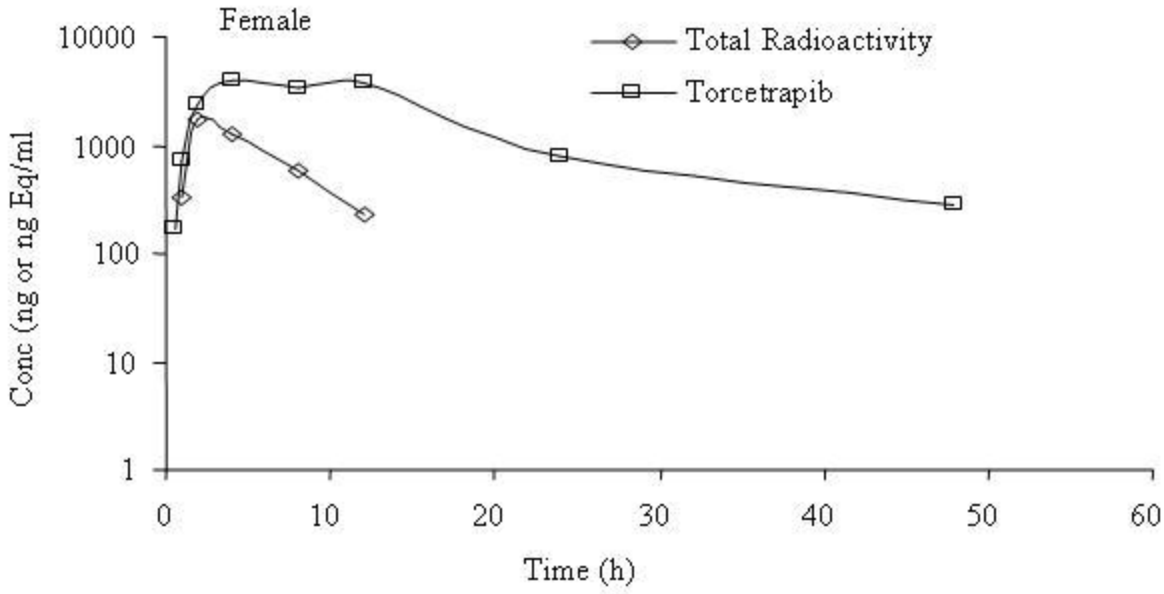
Female
Total Radioactivity
Torcetrapib
Conc (ng or ng Eq/ml
10000
1000
100
10
1
0
10
20
30
40
50
60
Time (h)

Fig. 2

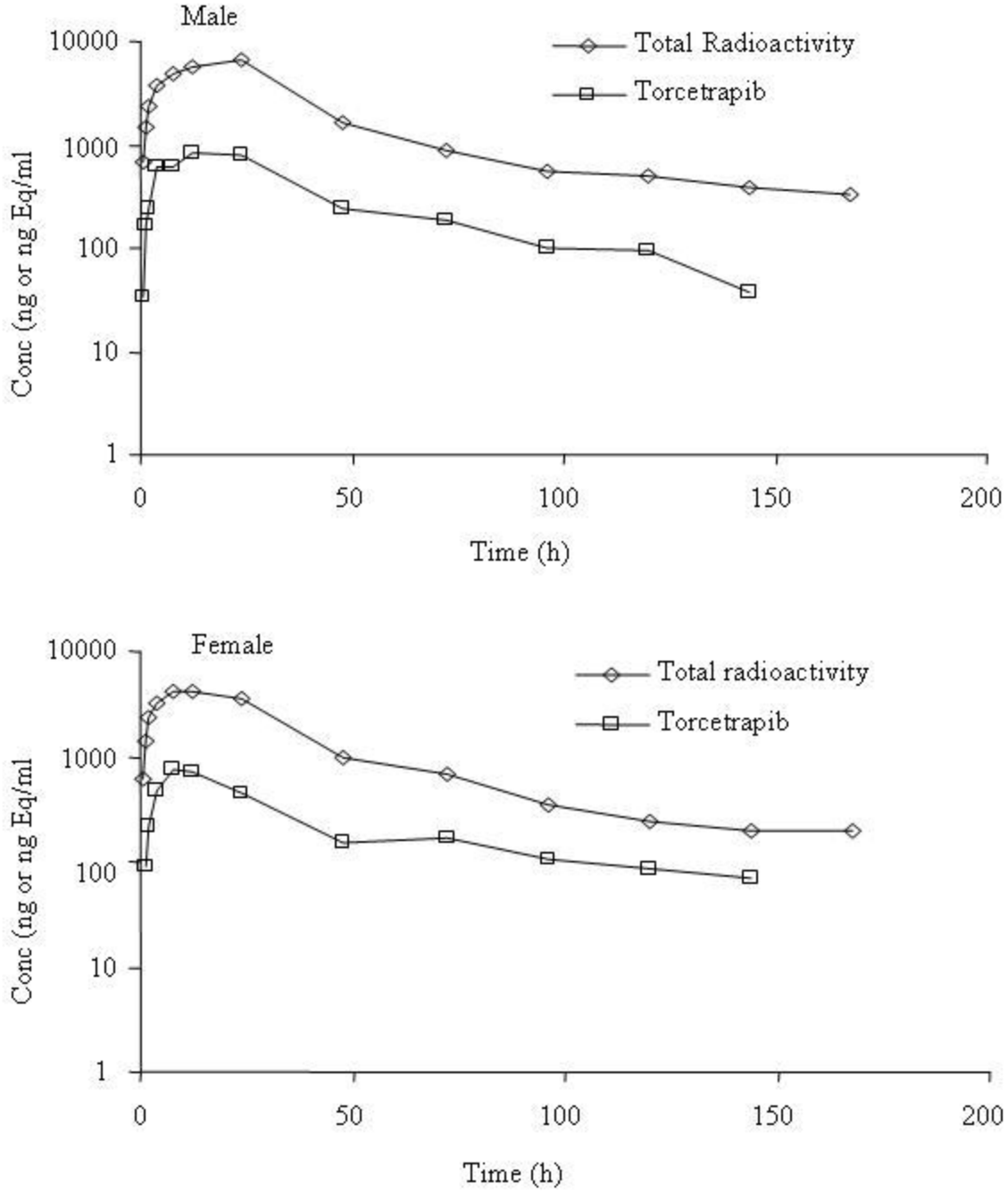
Male
Total Radioactivity
Torcetrapib
Conc (ng or ng Eq/ml
10000
1000
100
10
1
0
50
100
150
200
Time (h)
Female
Total radioactivity
Torcetrapib
Conc (ng or ng Eq/ml
10000
1000
100
10
1
0
50
100
150
200
Time (h)

Fig. 3

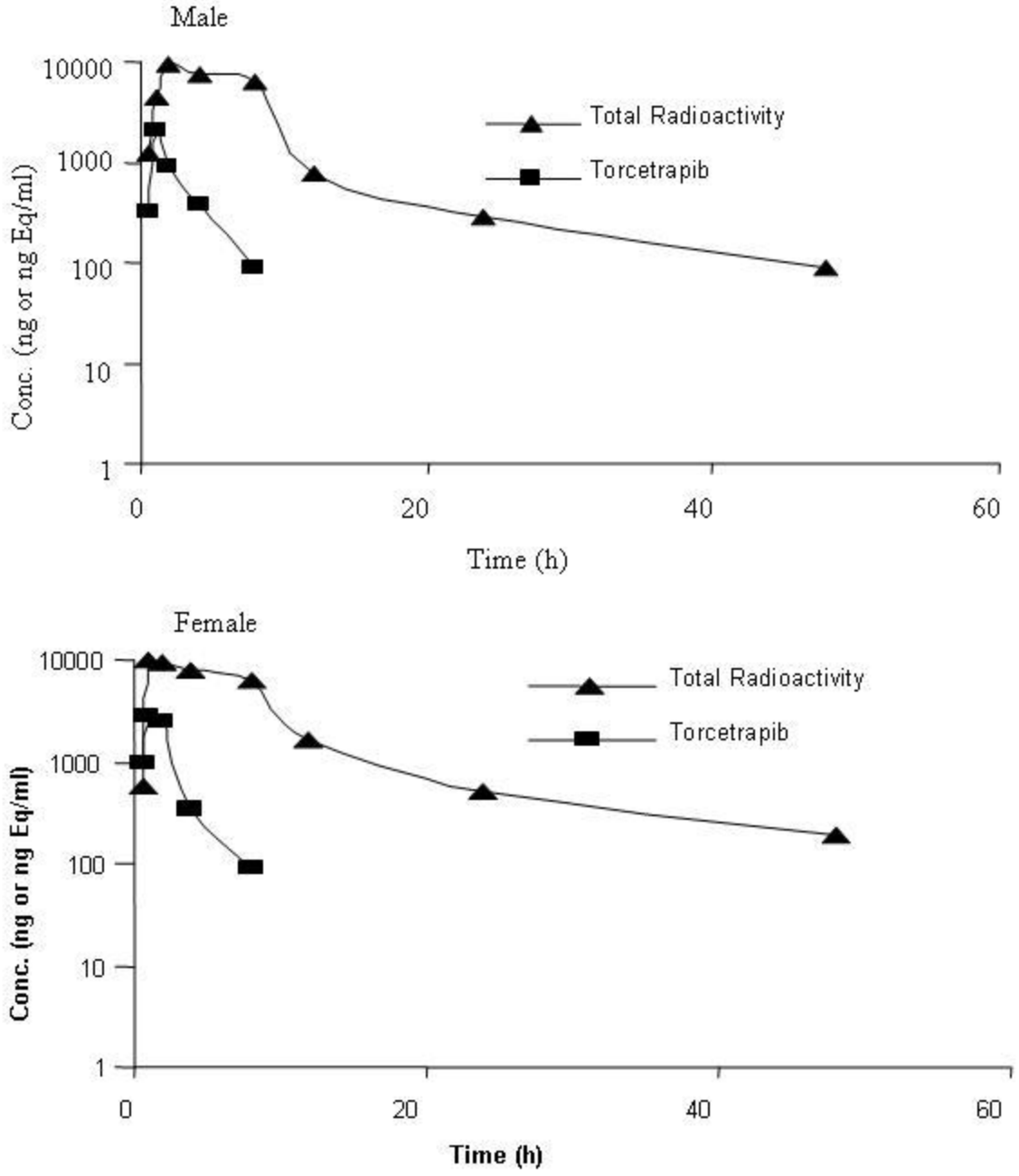
Male
10000
1000
100
10
1
Conc. (ng or ng Eq/ml)
Total Radioactivity
Torcetrapib
0
20
40
60
Time (h)

Female
10000
1000
100
10
1
Conc. (ng or ng Eq/ml)
Total Radioactivity
Torcetrapib
0
20
40
60
Time (h)

Fig. 4

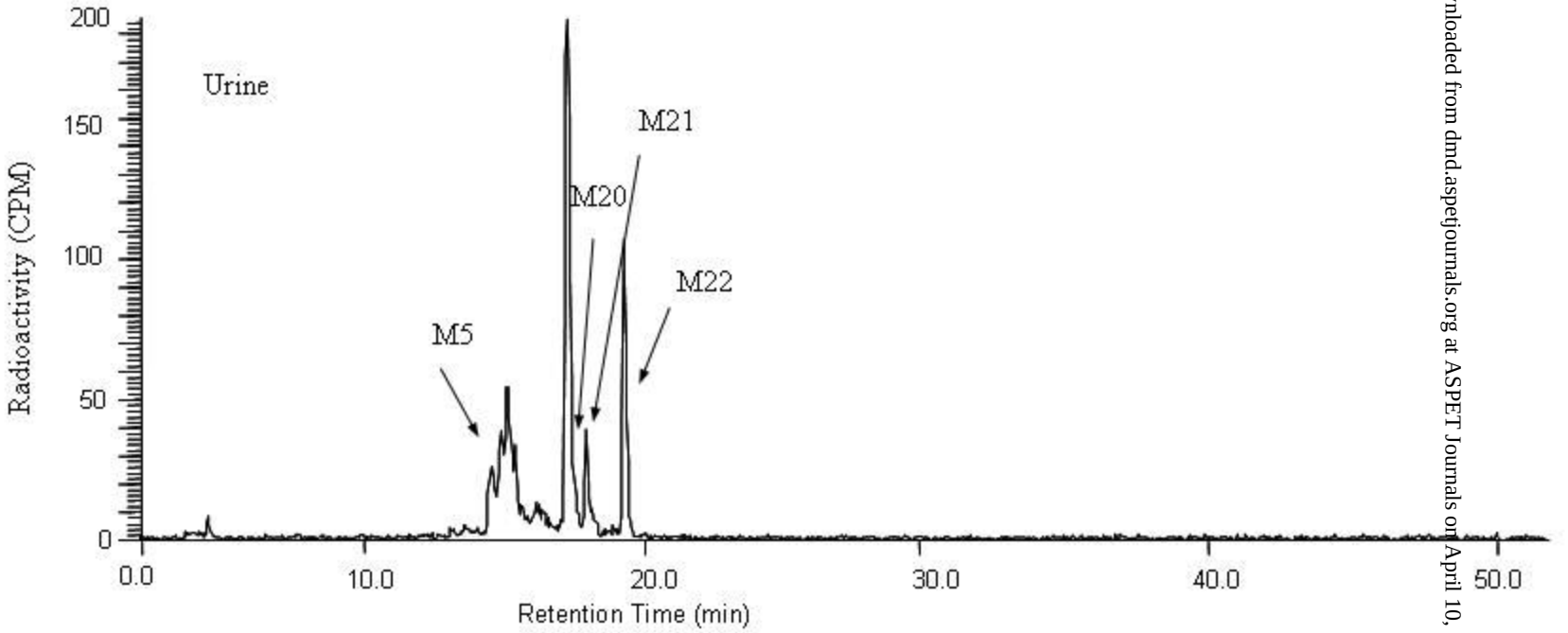

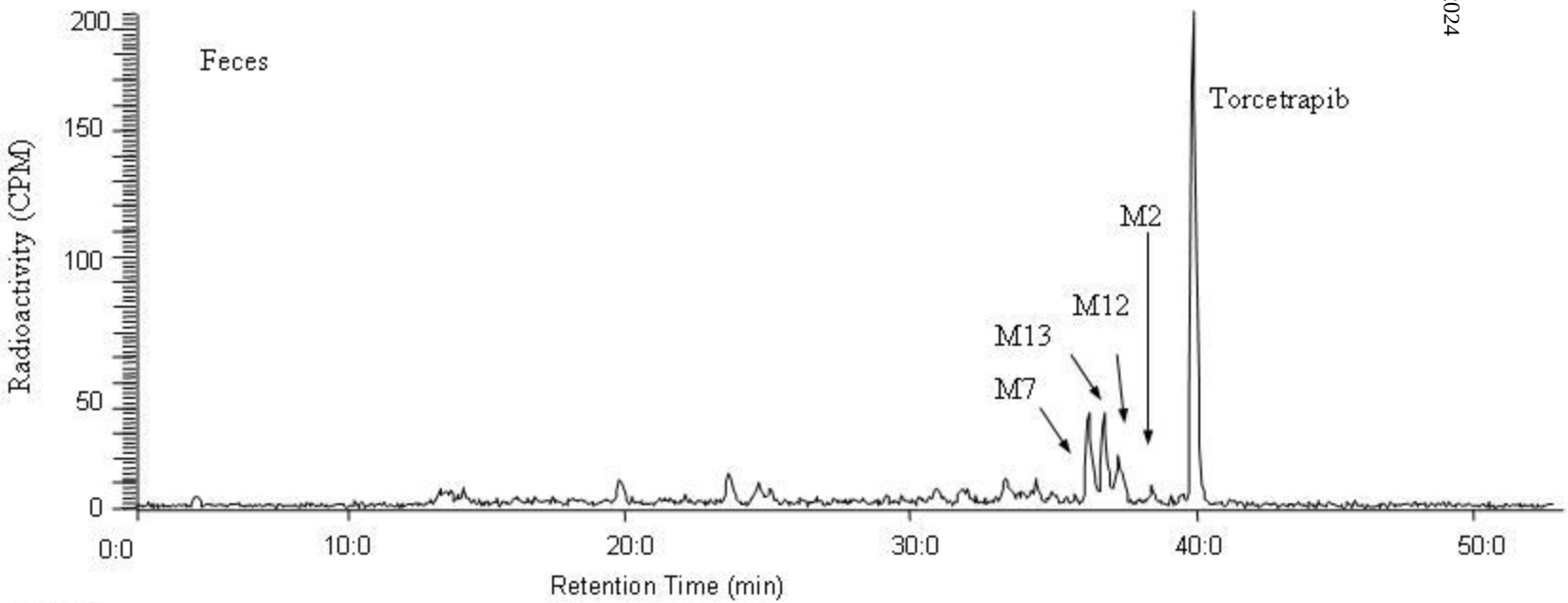

Fig. 5

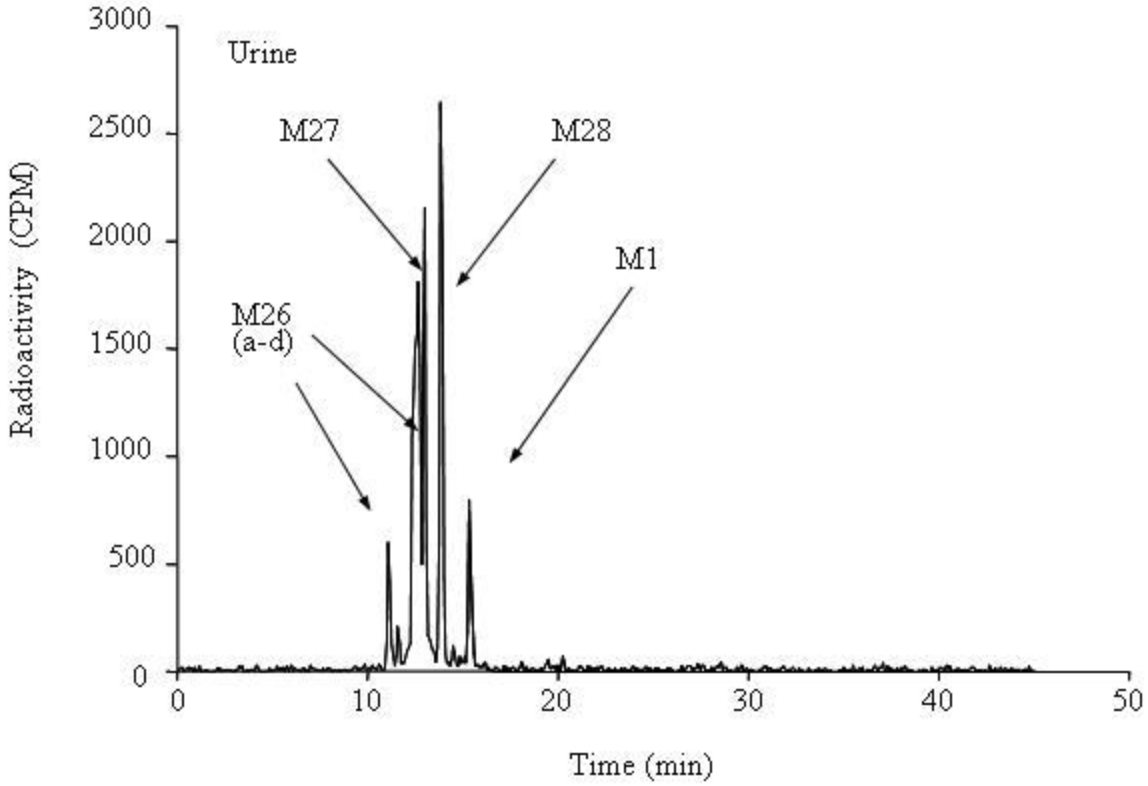
Urine
M27
M28
M1
M26
(a-d)
Radioactivity (CPM)
3000
2500
2000
1500
1000
500
0
0
10
20
30
40
50
Time (min)

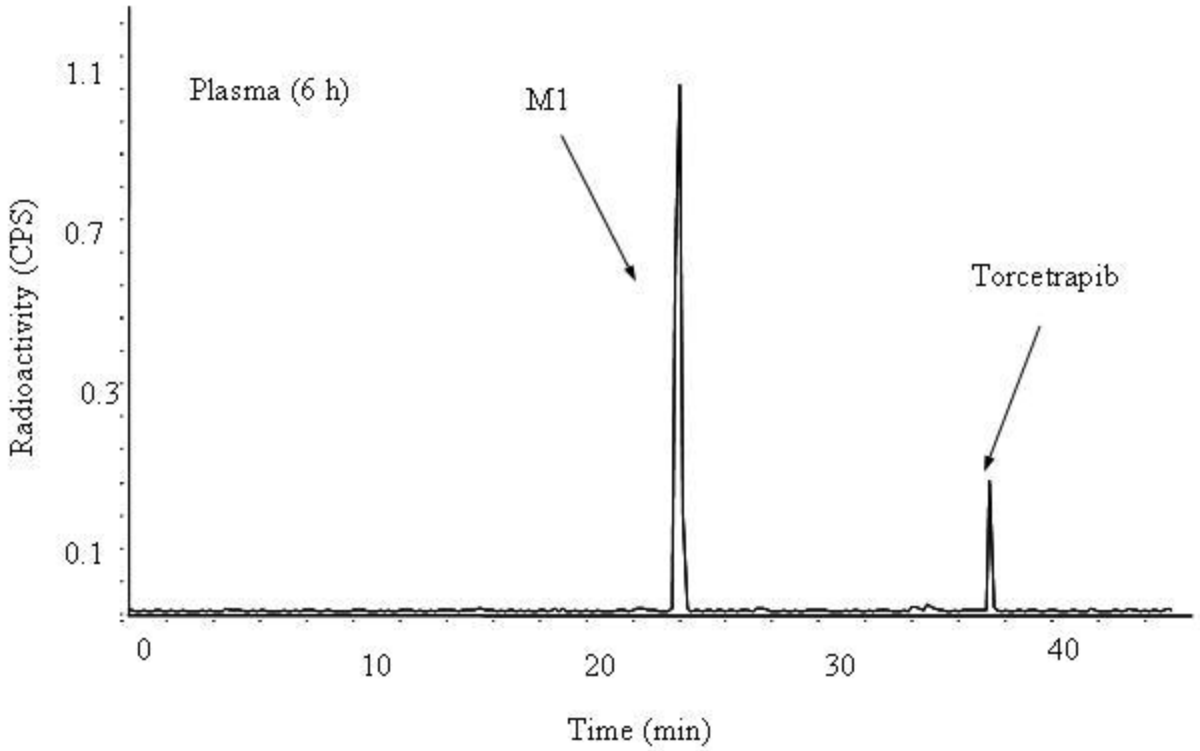
Plasma (6 h)
M1
Torcetrapib
Radioactivity (CPS)
1.1
0.7
0.3
0.1
0
10
20
30
40
Time (min)

Fig. 6

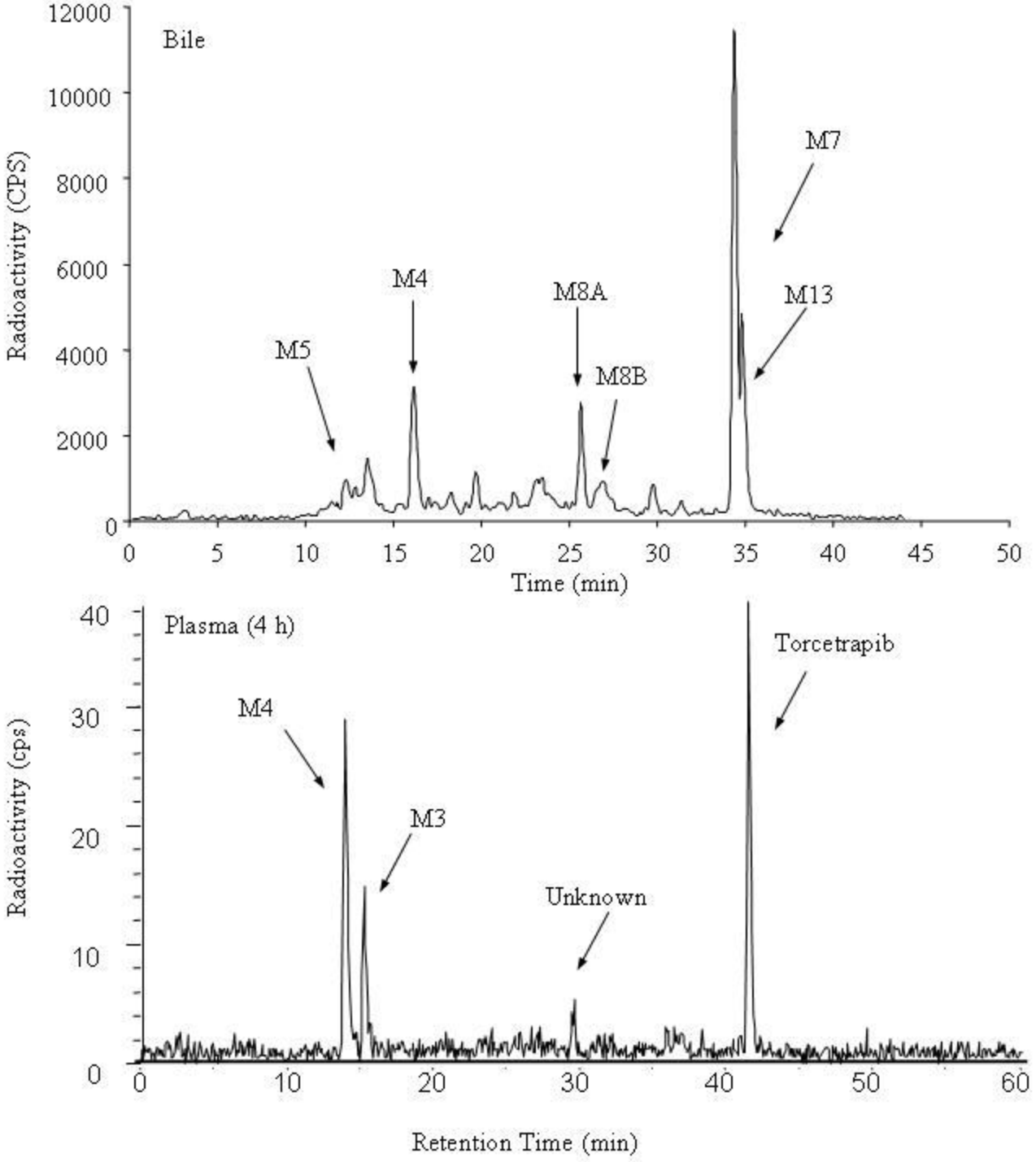
Bile
Radioactivity (CPS)
12000
10000
8000
6000
4000
2000
0
M5
M4
M8A
M8B
M7
M13
0
5
10
15
20
25
30
35
40
45
50
Time (min)
Plasma (4 h)
Radioactivity (cps)
40
30
20
10
0
M4
M3
Unknown
Torcetrapib
0
10
20
30
40
50
60
Retention Time (min)

Fig. 7

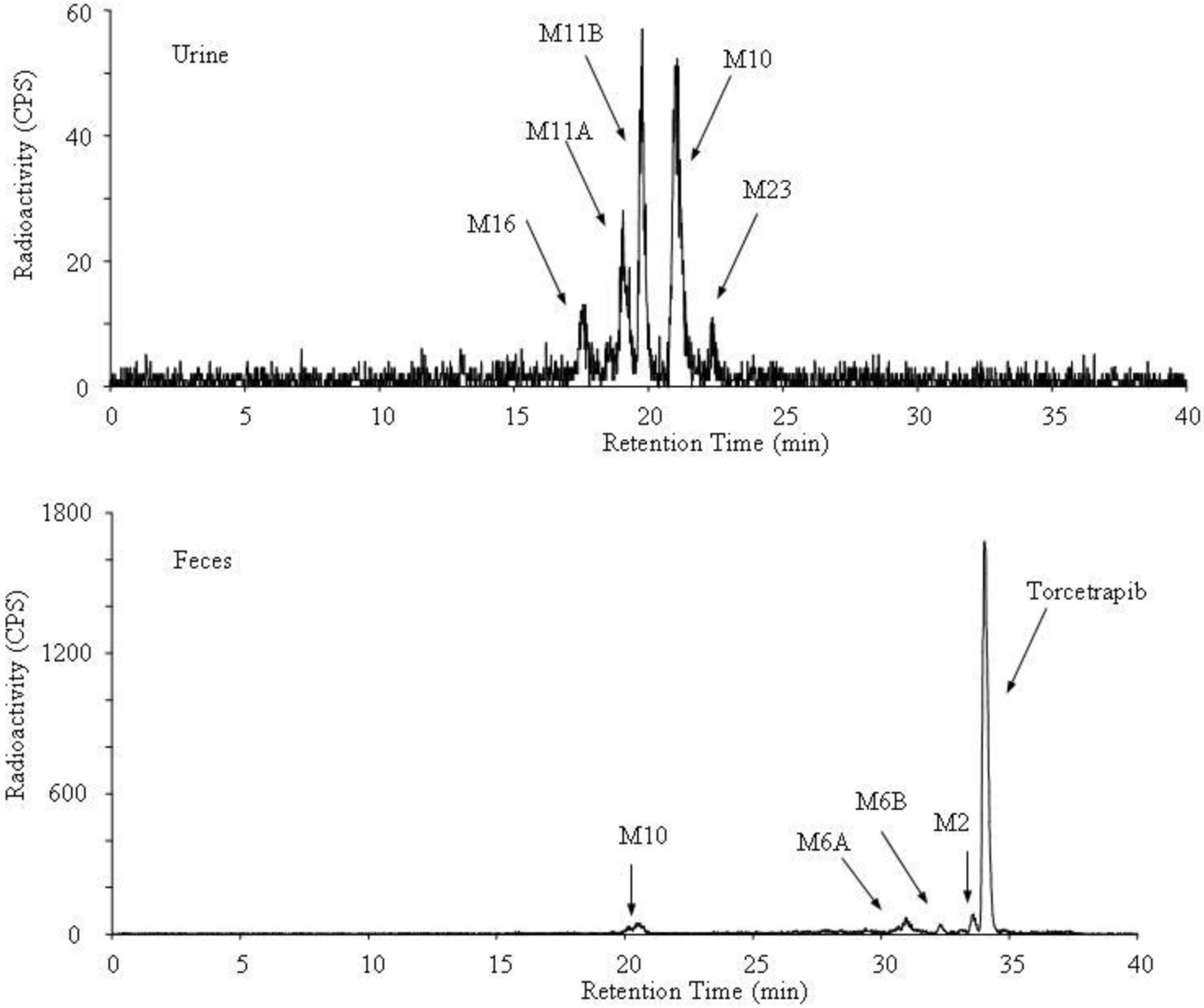

Fig. 8

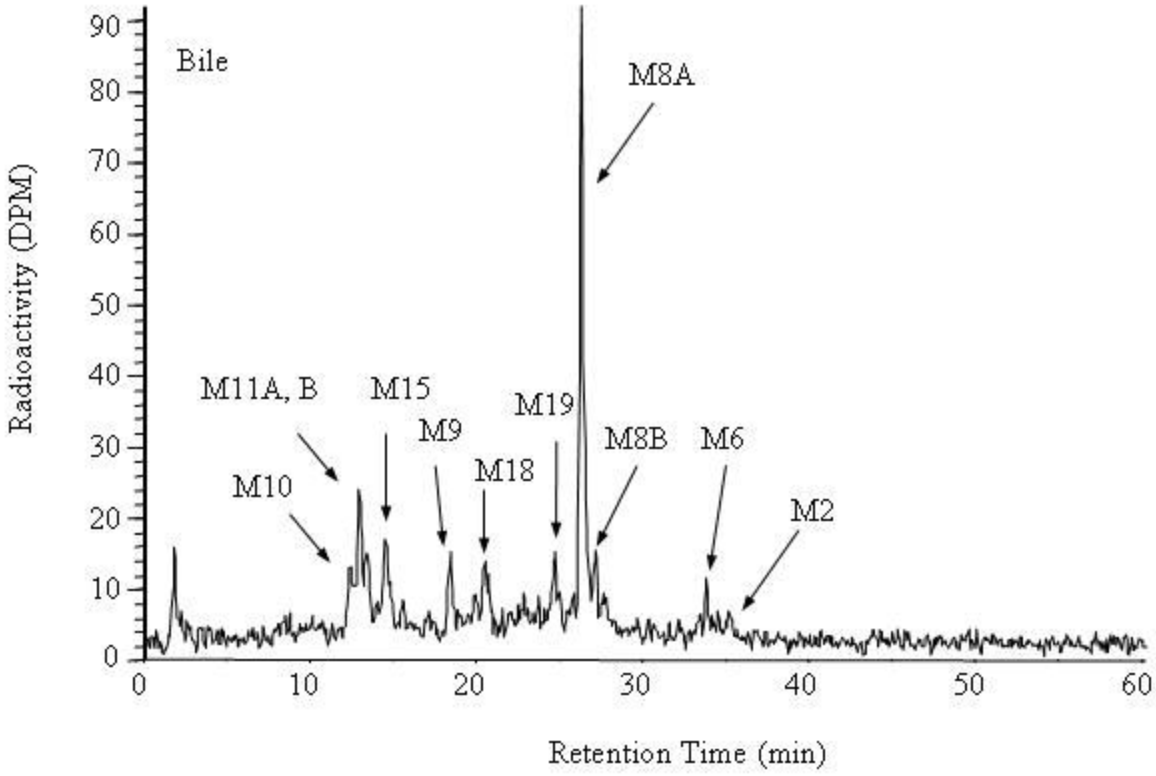
Bile
M8A
M11A, B
M15
M19
M9
M8B
M6
M10
M18
M2
Radioactivity (DPM)
Retention Time (min)
0
10
20
30
40
50
60
70
80
90

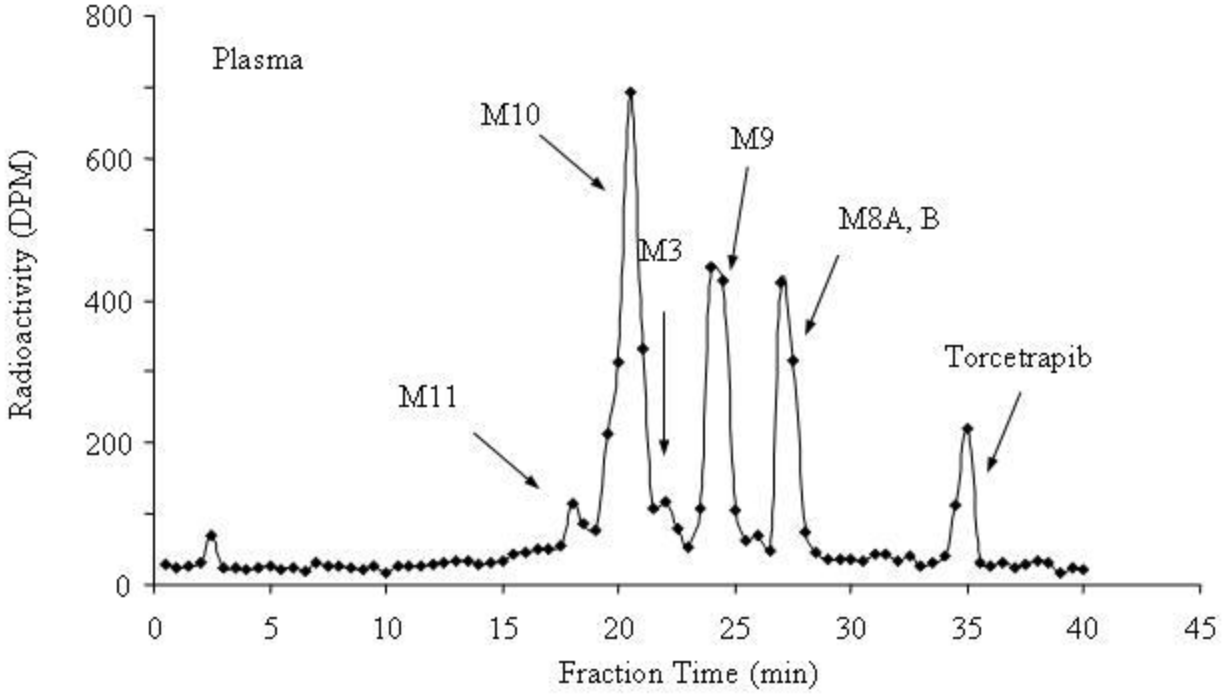
Plasma
M10
M9
M8A, B
M3
Torcetrapib
M11
Radioactivity (DPM)
Fraction Time (min)
0
200
400
600
800
0
5
10
15
20
25
30
35
40
45

Fig. 9

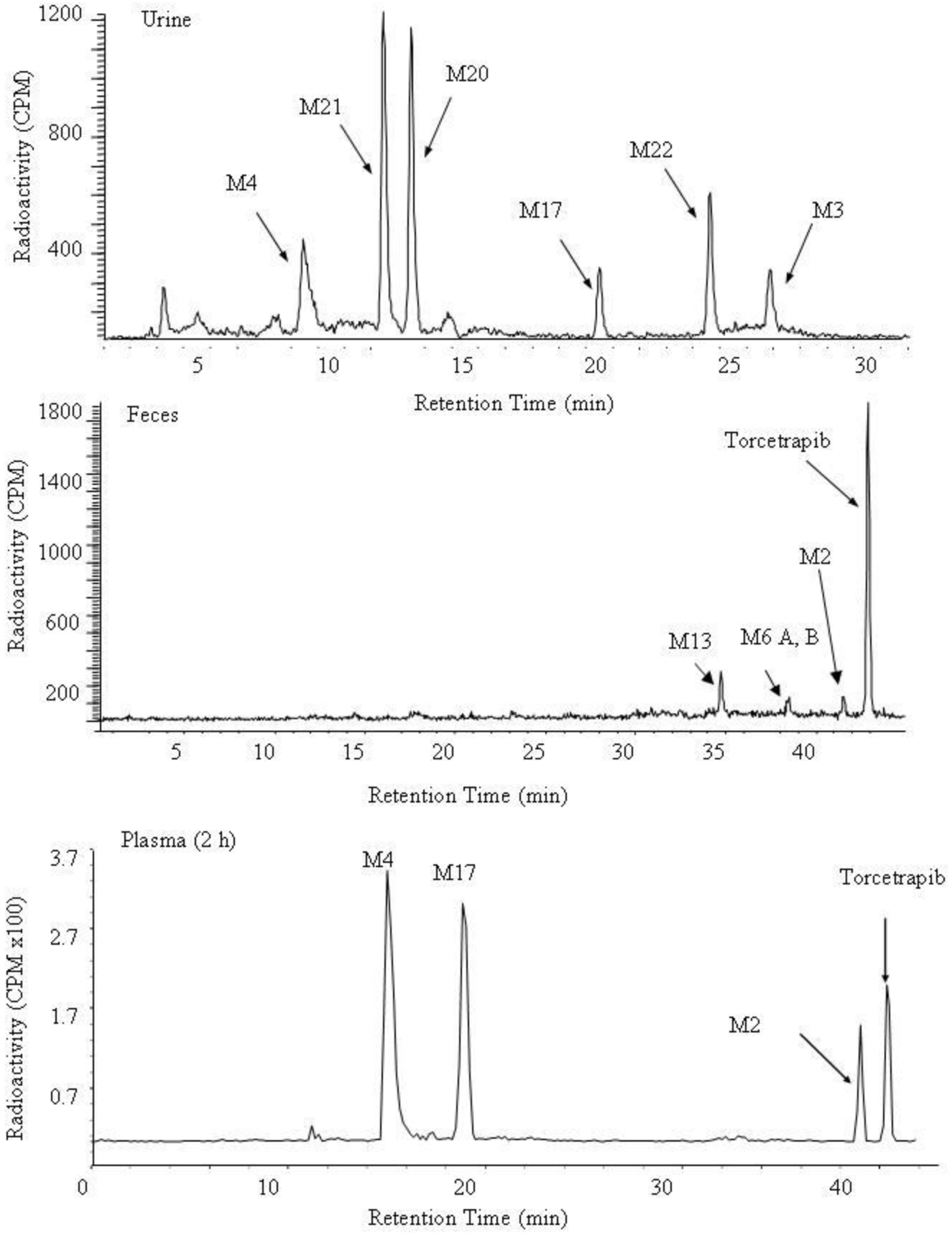
Urine
Radioactivity (CPM)
1200
800
400
M4
M21
M20
M17
M22
M3
5
10
15
20
25
30
Retention Time (min)
Feces
Radioactivity (CPM)
1800
1400
1000
600
200
Torcetrapib
M2
M13
M6 A, B
5
10
15
20
25
30
35
40
Retention Time (min)
Plasma (2 h)
Radioactivity (CPM x100)
3.7
2.7
1.7
0.7
M4
M17
Torcetrapib
M2
0
10
20
30
40
Retention Time (min)

Fig. 10

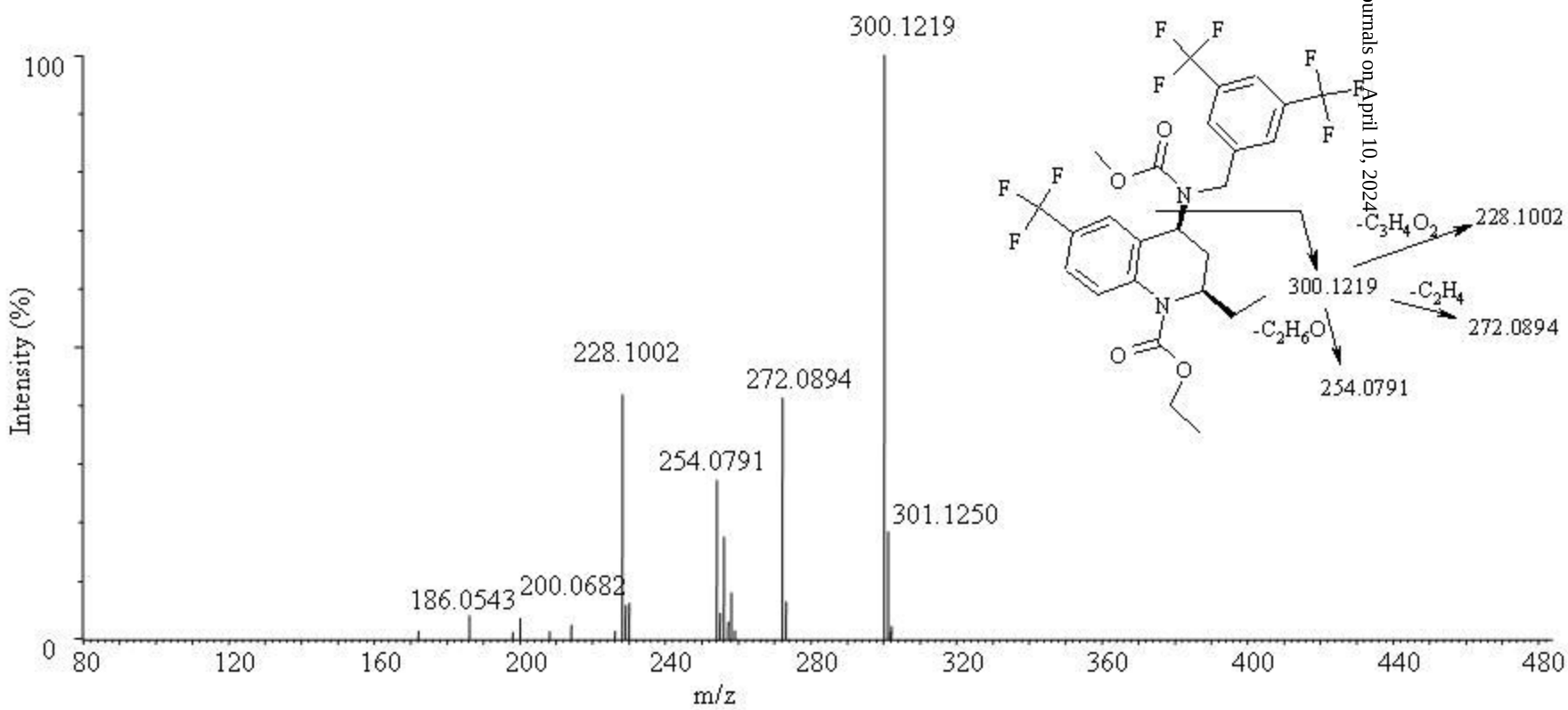

Fig. 11

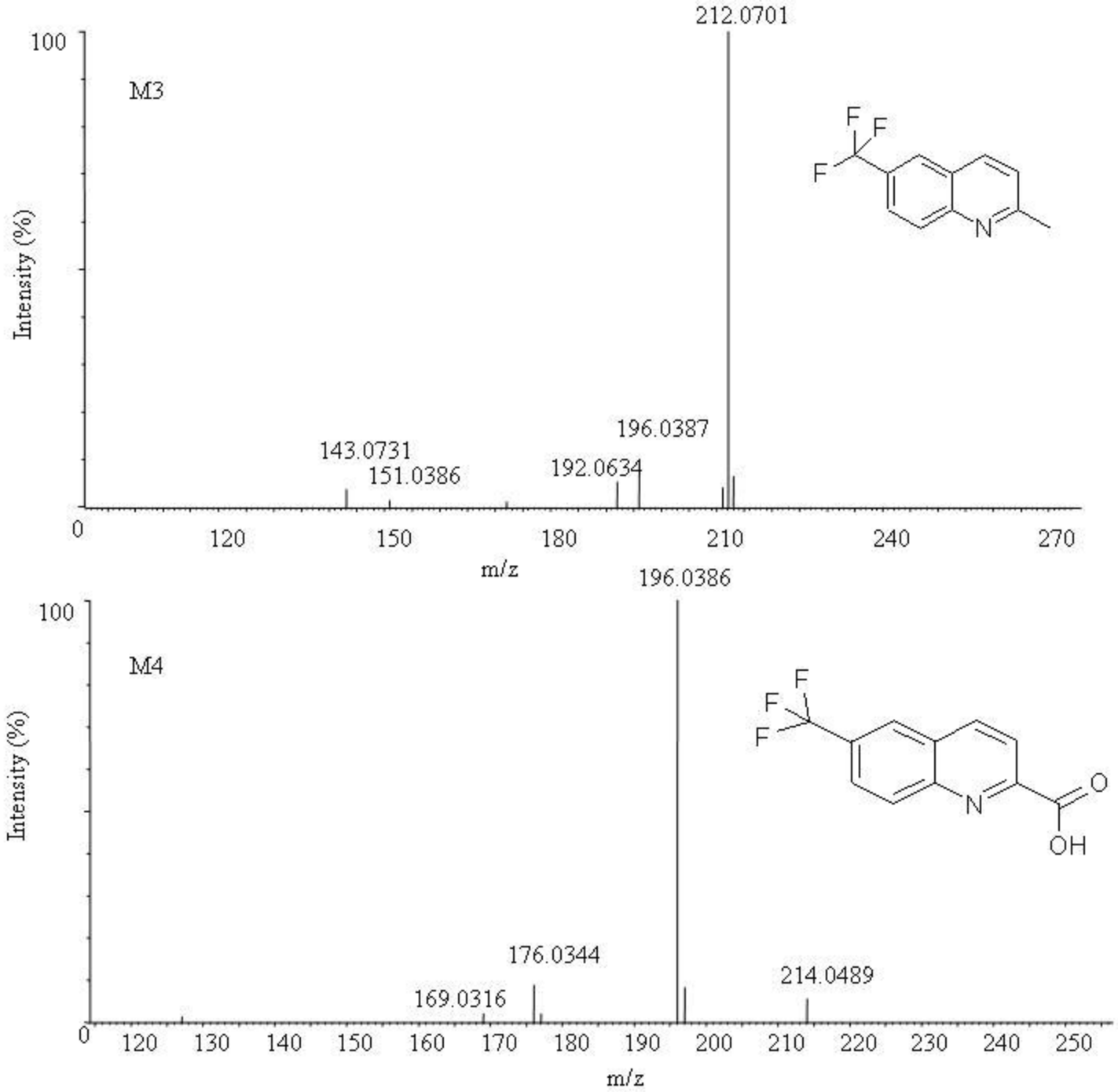

Fig. 12

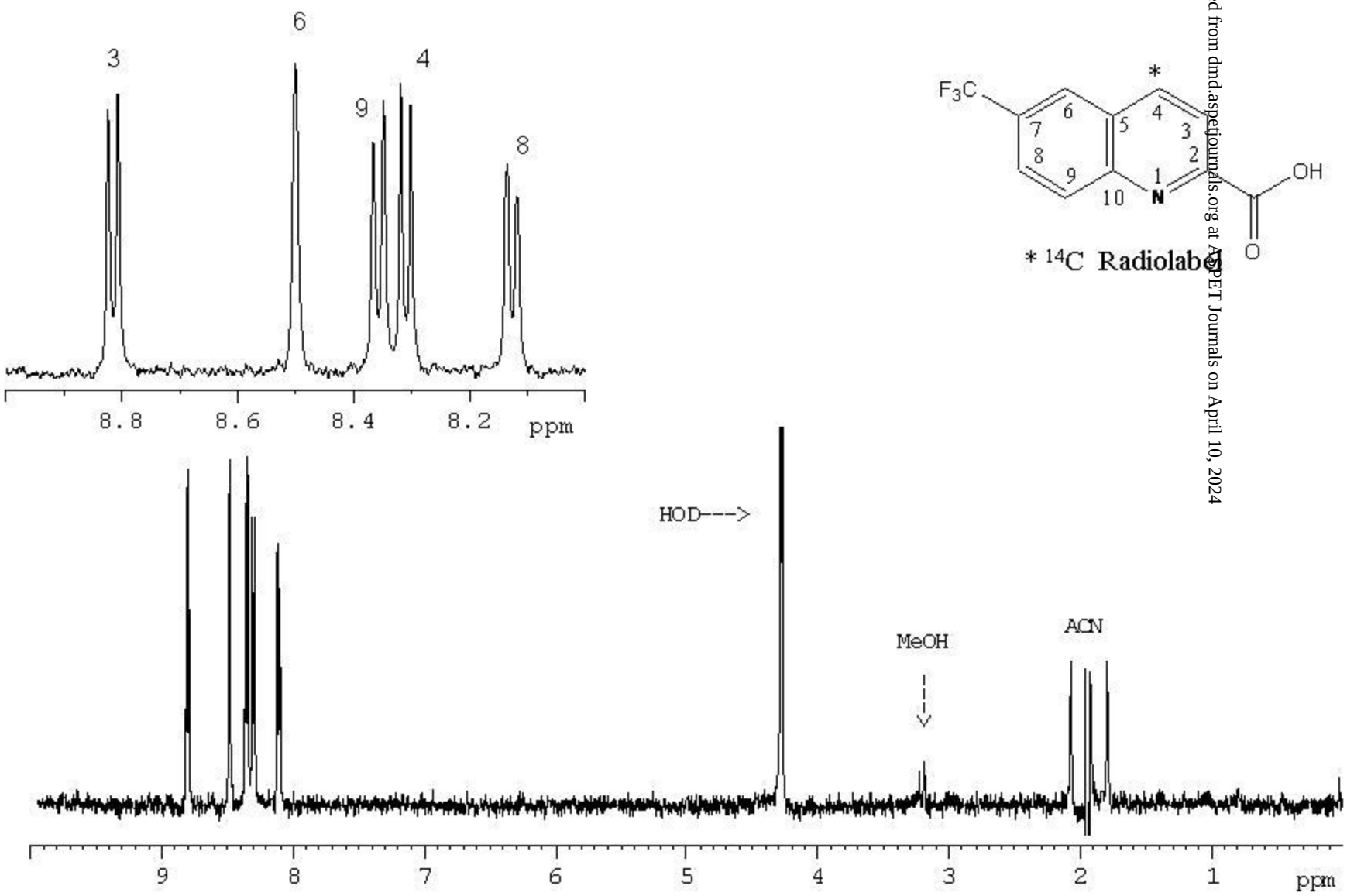

Fig. 13

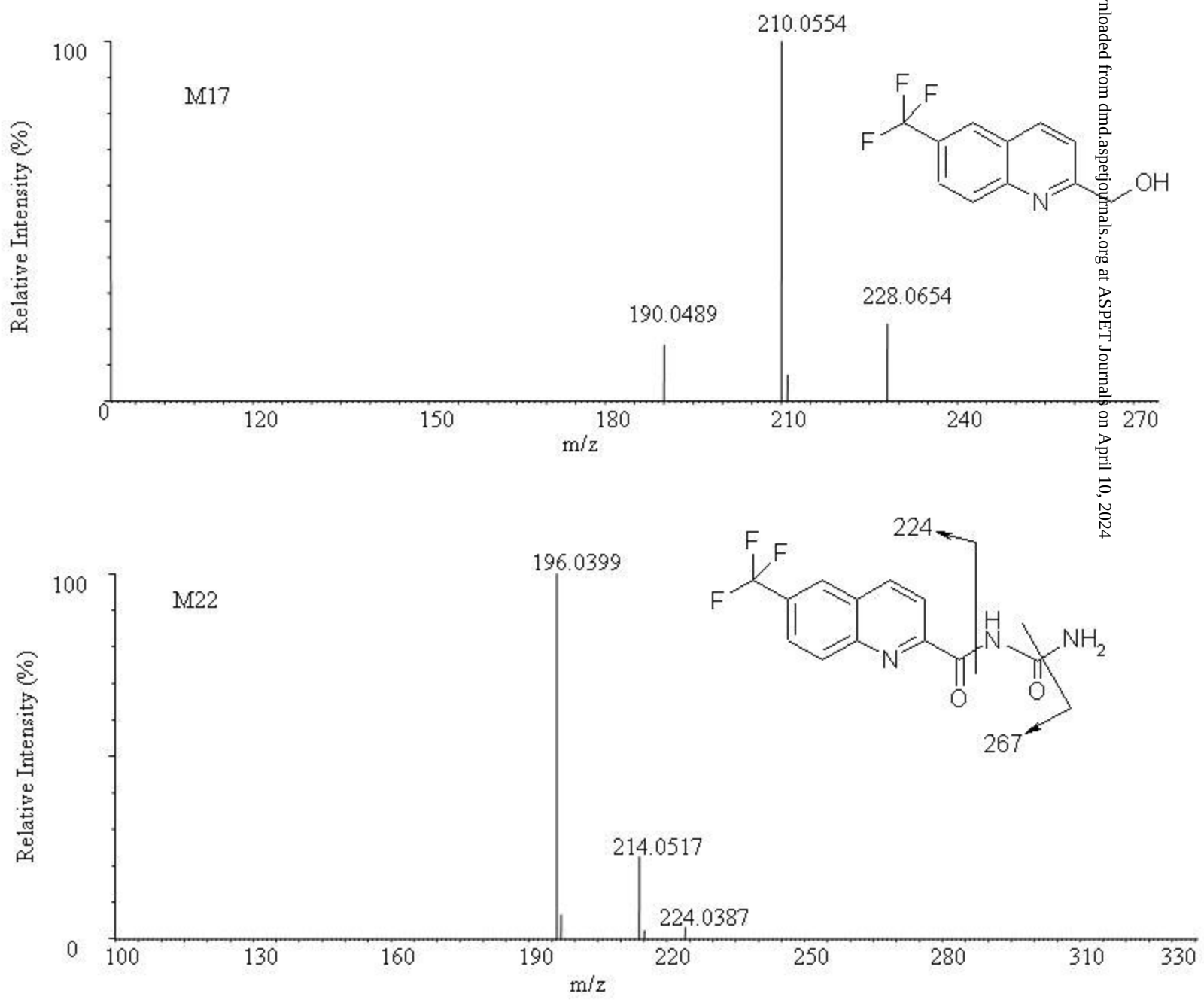

Fig. 14

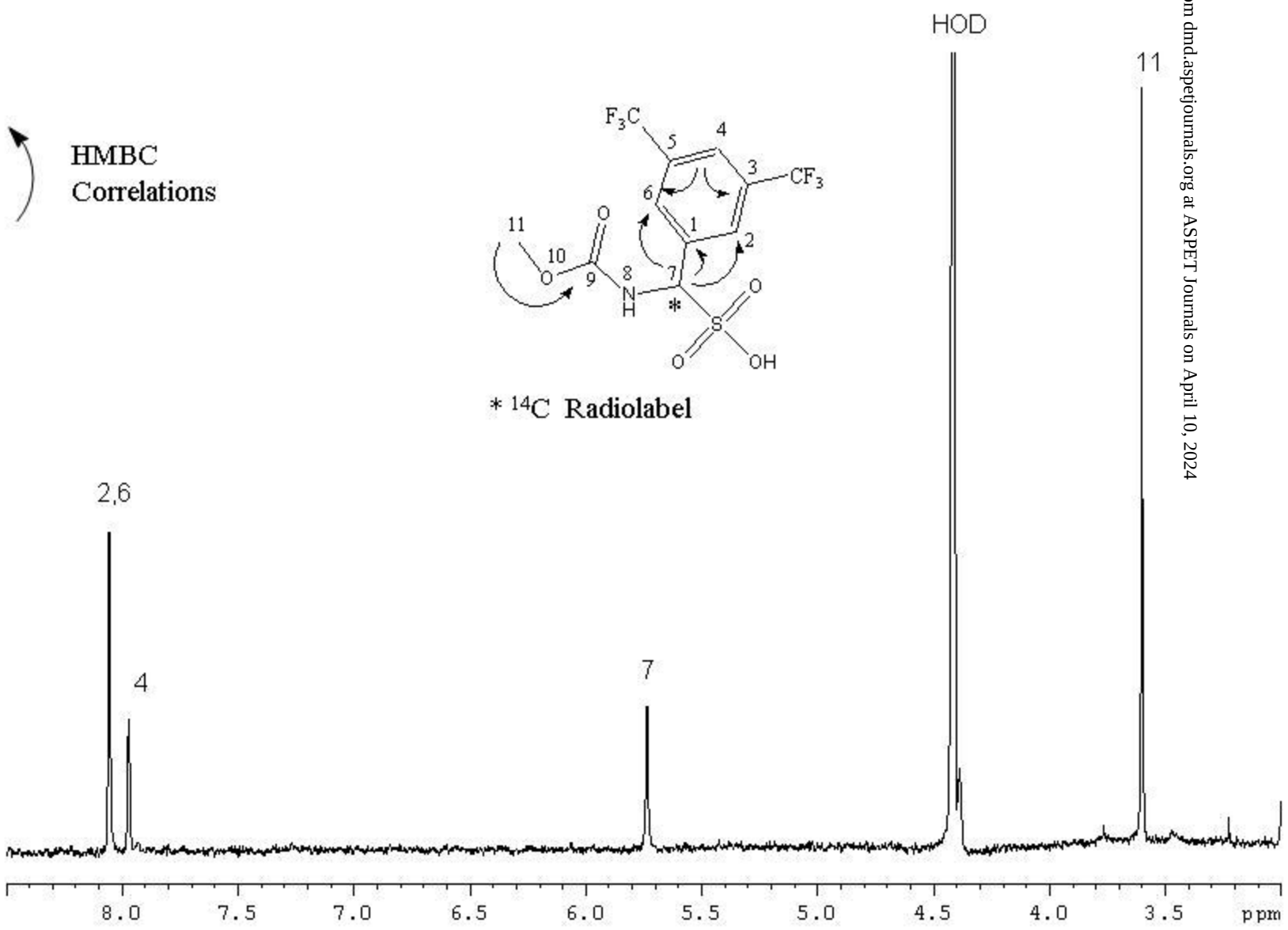

Fig. 15

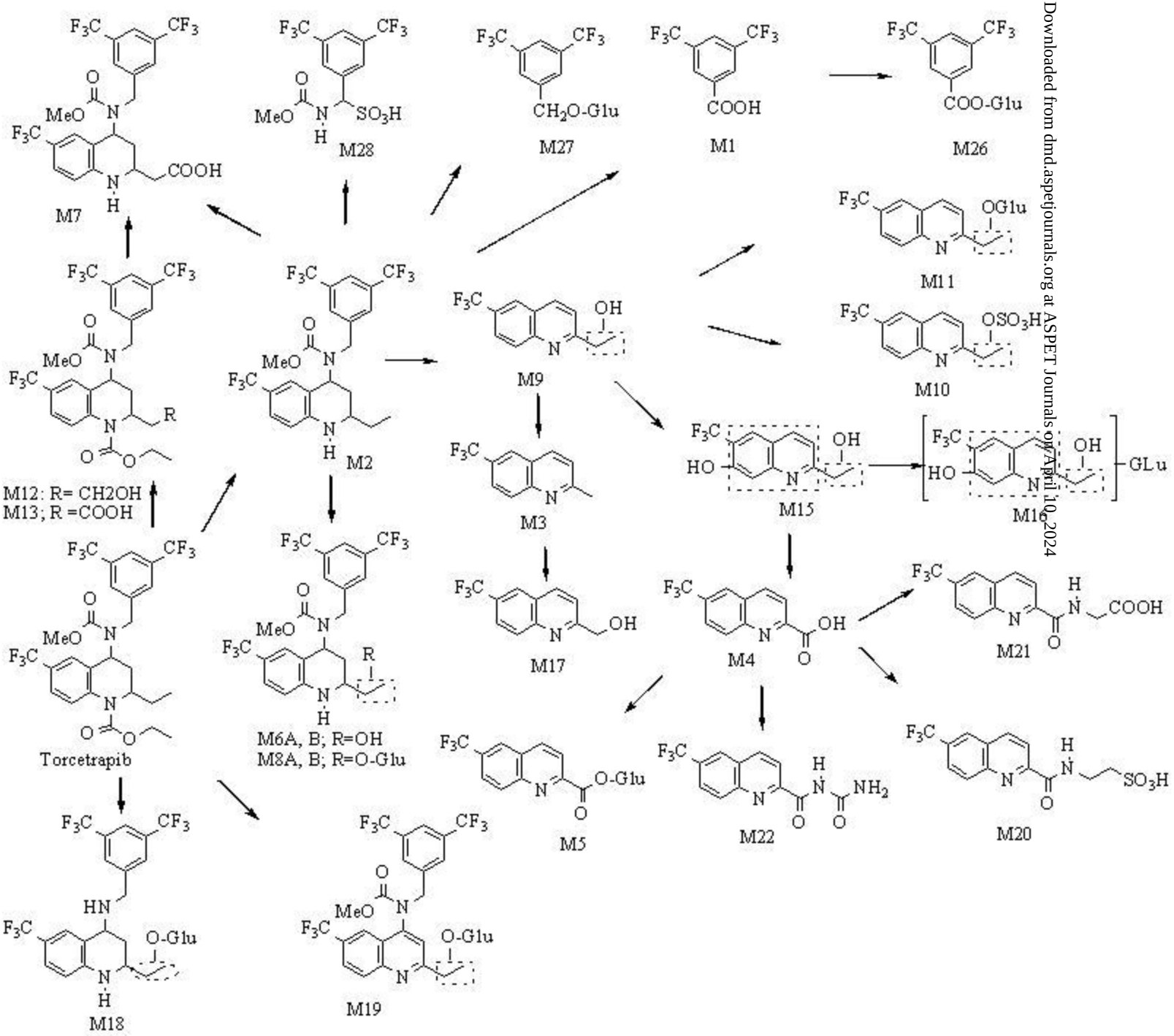

Fig. 16

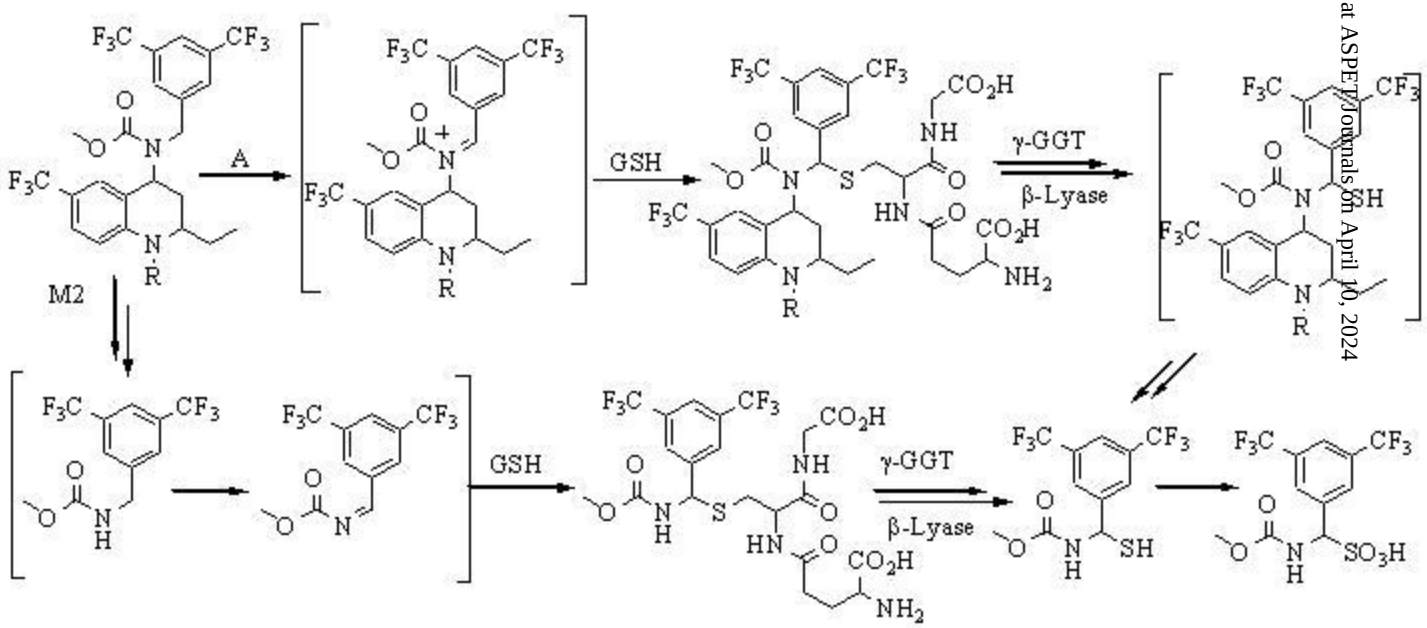

Fig. 17